NATIONAL ENERGY TECHNOLOGY LABORATORY OIL & GAS

DOE Award No.: DE-FE0023919

Phase 4 Scientific/Technical Report

Type: Other
Project Period 4: 10/01/2019 to 09/30/2020

Deepwater Methane Hydrate Characterization and Scientific Assessment

Submitted by:
Peter B. Flemings

Signature

The University of Texas at Austin
DUNS #:170230239
101 East 27th Street, Suite 4.300
Austin, TX 78712
Email: pflemings@jsg.utexas.edu
Phone number: (512) 475-8738

Prepared for:
United States Department of Energy
National Energy Technology Laboratory

March 02, 2021

U.S. DEPARTMENT OF ENERGY | NATIONAL ENERGY TECHNOLOGY LABORATORY

Office of Fossil Energy

DISCLAIMER

This report was prepared as an account of work sponsored by an agency of the United States Government. Neither the United States Government nor any agency thereof, nor any of their employees, makes any warranty, express or implied, or assumes any legal liability or responsibility for the accuracy, completeness, or usefulness of any information, apparatus, product, or process disclosed, or represents that its use would not infringe privately owned rights. Reference herein to any specific commercial product, process, or service by trade name, trademark, manufacturer, or otherwise does not necessarily constitute or imply its endorsement, recommendation, or favoring by the United States Government or any agency thereof. The views and opinions of authors expressed herein do not necessarily state or reflect those of the United States Government or any agency thereof.

ABSTRACT

This is the Phase 4 Report for the 'Deepwater Methane Hydrate Characterization and Scientific Assessment or Genesis of Methane Hydrates in the Gulf of Mexico (GOM2)' research project (DOE Award No. DE-FE0023919). The report summarizes activities from October 1, 2019 to September 30, 2020. The project is led by the University of Texas at Austin (UT). The project objective is to gain insight into the nature, formation, occurrence and physical properties of methane hydrate-bearing sediments for the purpose of methane hydrate resource appraisal through the planning and execution of drilling, coring, logging, testing and analytical activities that assess the geologic occurrence, regional context, and characteristics of marine methane hydrate deposits in the Gulf of Mexico outer continental shelf (OCS). Our most important results are listed below.

1. **AAPG Volume 1 Publication:**
    - We published a dedicated American Association of Petroleum Geologists Bulletin volume describing initial results from the UT-GOM2-1 expedition in Sept. 2020. This is part 1 of a multi-volume commitment by AAPG to this project (Section 4.1).
2. **GOM2-1 Core Analysis:**
    - We further confirmed that the natural gas in hydrate at GC-955 was formed by primary microbial processes (>76.1 %) (Section 3.2).
    - The in-situ effective permeability hydrate-bearing sandy silts at the GC-955 reservoir ranges from 0.1 md (1.0×10^{-16} m^2) to 2.4 md ($2.4\times10^{-15}m^2$) in cores with 83% to 93% hydrate saturation. The intrinsic permeability (the single phase permeability) is estimated from reconstituted samples to be ~12 md (1.2×10^{-14} m^2) to ~41 md (4.1×10^{-14} m^2) (Section 3.2).
    - We used observation and models to interpret that the core degradation that is found in pressure cores is due to dissociation of the methane hydrate in the outer circumference of the core and dissolution of that methane into the fresh pore water that the core is stored with. We are designing approaches to minimize this core loss in the future (Section 3.2).
3. **Pressure Coring Technology Advancement:**
    - We spent an enormous amount of effort to further improve the ability of the pressure coring tool (the PCTB) to pressure seal correctly.
    - Upper Section Modification: We completed upgrading the upper section of the PCTB to address poor pressure (Section 3.6.1).
    - Bench Test Upper Section: We successful tested the modifications at Geotek's test facility in Salt Lake City (Bench Test II) (Section 3.6.2).
    - PCTB Land Test: We completed a Land Test of the PCTB at the Schlumberger Cameron Test and Training Facility (CTTF). The tool did not seal in 6 out of 7 tests, and we clearly demonstrated that cuttings were wedging in the ball valve assembly, keeping the ball valve from sealing (Section 3.6.3).
    - Further PCTB Testing & Modifications: We reproduced the failure mechanism observed during the land test at Salt Lake City and confirmed the sensitivity of the ball valve assembly to grit. Geotek designed and tested 9 modifications to address this issue and the PCTB is now 100% successfully sealing in the presence of grit. (See Section 3.6.4).
4. **Preparation for UT-GOM2-2:**

- Our science expedition is scheduled for spring 2022 and we are fully focused on preparing for this.
- Shallow Hazard Assessment: UT and Ohio State completed a Shallow Hazard Assessment report for each proposed UT-GOM2-2 drilling location, pursuant to 30 CFR 250.214(f) and 250.244 (f). The Shallow Hazard Reports will accompany the UT-GOM2-2 Exploration Plan that is submitted to BOEM, and completes the geological and geophysical analysis for UT-GOM2-2 permitting efforts (See Section 3.7.1)
- Operations Plan: We updated the UT-GOM2-2 Operations Plan (Version 1). We completed the UT-GOM2-2 Science and Sample Distribution Plan (Version 1) (See Section 3.3)
- Vessel Selection: We evaluated the scope, budget, and schedule that would result from using a commercial vessel. We developed detailed drilling schedule, mud volume, and resource estimates. We developed a vessel specification document and a well plan, and sent these documents to prospective vessel contractors. (See Section 3.4)

TABLE OF CONTENTS

DISCLAIMER ii

ABSTRACT iii

TABLE OF CONTENTS v

LIST OF TABLES vii

LIST OF FIGURES viii

1 EXECUTIVE SUMMARY 1

2 INTRODUCTION 3

3 SUMMARY OF PHASE 4 TASKS 5

3.1 Task 1.0: Project Management and Planning 6

3.2 Task 10.0: Pressure Core Analysis 8

3.2.1 Subtask 10.4: Continued Pressure Core Analysis (UT-GOM2-1) 8

3.2.2 Subtask 10.5: Continued Hydrate Core-Log-Seismic Synthesis (UT-GOM2-1) 22

3.2.3 Subtask 10.6: Additional Core Analysis Capabilities 22

3.2.4 Subtask 10.7: Hydrate Modeling 23

3.3 Task 11.0: Update Science and Operational Plans for UT-GOM2-2 31

3.3.1 UT-GOM2-2 Operations Plan 31

3.3.2 UT-GOM2-2 Science and Sample Distribution Plan 32

3.4 Task 12.0: UT-GOM2-2 Scientific Drilling Program Vessel Access 33

3.5 Task 13.0: Maintenance and Refinement of Pressure Core Transport, Storage, and Manipulation Capability 35

3.5.1 Subtask 13.1: Hydrate Core Manipulator and Cutter Tool 35

3.5.2 Subtask 13.2: Hydrate Core Effective Stress Chamber 36

3.5.3 Subtask 13.3: Hydrate Core Depressurization Chamber 37

3.5.4 Subtask 13.4: Develop Hydrate Core Transport Capability for UT-GOM2-2 38

3.5.5 Subtask 13.5: Expansion of Pressure Core Storage Capability for UT-GOM2-2 38

3.5.6 Subtask 13.6: Continued Storage of Hydrate Cores from UT-GOM2-1 Marine Field Test 38

3.5.7 Subtask 13.7: X-ray Computed Tomography 39

3.5.8 Subtask 13.8: Pre-consolidation System 39

3.6 Task 14.0: Performance Assessment, Modifications, and Testing of PCTB 40

3.6.1 Subtask 14.2: PCTB Modifications/Upgrades 40

3.6.2 Subtask 14.1: PCTB Lab Test 41

3.6.3 Subtask 14.3: PCTB Land Test II 42

3.6.4 Other: Post-Land Test Evaluation, Testing, and Modification 47
3.7 Task 15.0: UT-GOM2-2 Scientific Drilling Program Preparations 50
3.7.1 Subtask 15.3: Permitting for UT-GOM2-2 Scientific Drilling Program 50
4 PRODUCTS DEVELOPED 51
4.1 AAPG Special Volume on GC 955, Gulf of Mexico 51
4.2 UT-GOM2-1 Scientific Report 53
4.3 Publications 53
4.4 Conference Presentations / Abstracts 56
4.5 Websites or other Internet Sites 61
4.6 Other Products 61
5 ACRONYMS AND ABBREVIATIONS 62
6 BIBLIOGRAPHY 64

LIST OF TABLES

Table 3-1: Summary of Phase 4 tasks 5
Table 4-1: AAPG Special Volume on GC 955, Gulf of Mexico, papers and DOI links 52
Table 4-2: UT-GOM2-1 Scientific Volume 53
Table 5-1: List of Acronyms and Abbreviations 62

LIST OF FIGURES

Figure 3-1: Image of inflatable bag attached to the quantitative degassing manifold 9
Figure 3-2: Scatter plots of C_1/C_2+ versus $\delta^{13}C$-CH_4 (top, A) and a zoomed in plot of just UT-GOM2-1 samples (bottom, B) 11
Figure 3-3: Scatter plot of δ^2H-CH_4 vs. $\delta^{13}C$-CH_4 (top, A) and zoomed in (bottom, B) 12
Figure 3-4: Scatter plot of $\delta^{13}C$-CO_2 vs. $\delta^{13}C$-CH_4 (top, A) and zoomed in (bottom, B) 13
Figure 3-5: A summary of effective permeabilities of UT-GOM2-1 hydrate bearing sandy silt sediment from pressure core sections as a function of vertical effective stress. 14
Figure 3-6: Photo and CT image of core 7FB3-04 after hydrate dissociation. 15
Figure 3-7: Permeability of UT-GOM2-1 Sandy silt sediment from three pressure core sections as a function of vertical effective stress before (effective permeability). 16
Figure 3-8: micro-Raman spectrometer set up in the UT Pressure Core Center 17
Figure 3-9: Two-dimensional Raman maps of a pressure core from the Gulf of Mexico. 18
Figure 3-10: Images of the bottom 77 cm of core section H005-05FB-3 from before and after storage. 19
Figure 3-11: Sorting of all Bulk and Organic Carbon-Free GOM2-1 samples plotted against their median grain size (Phi units) from measurements of grain size completed at UNH using laser diffraction. 21
Figure 3-12: Schematic diagram of the response to a pressure perturbation of a hydrate-bearing sample during isothermal dissociation (from point a to point b) and endothermically dissociation without heat flow (from point a to point c) followed by a shut-in interval. 23
Figure 3-13: Schematic of the 2D radial model for pressure recovery during a shut-in period when a hydrate-bearing core is depressurized. 26
Figure 3-14: Evolution of (a) pressure and (b) temperature at 2.0 cm from the top of the chamber (blue lines) and 1.69 cm from the top of hydrate-bearing sediment (red lines) during a shut-in period. (c) 28
Figure 3-15: Dissolved methane concentration (a, b), salinity (c, d) and hydrate saturation (e, f) at the initial condition and after 15 months of storage at 24 MPa and 6.0 ^oC. 30
Figure 3-16: Methane hydrate phase diagram for different salinities. 32
Figure 3-17: Core CTTF-02FB contained 8.9 ft of limestone and shale after recovery (91% recovery). 43
Figure 3-18: DST and rig instrumentation plots for core CTTF-01FB. 44
Figure 3-19: Partially closed ball valve after recovery from the hole. 45
Figure 3-20: Apparently closed ball valve upon recovery from the hole. 45
Figure 3-21: Geotek testing facility in Salt Lake City, Utah. 47
Figure 3-22. Cross sectional view of the PCTB ball valve assembly. 48
Figure 4-1: AAPG Bulletin, Vol. 104 Number 9, September 2020 51

1 EXECUTIVE SUMMARY

This is the Phase 4 Report for the 'Deepwater Methane Hydrate Characterization and Scientific Assessment or Genesis of Methane Hydrates in the Gulf of Mexico (GOM2)' research project (DOE Award No. DE-FE0023919). It summarizes activities from October 1, 2019 to September 30, 2020.

The project is led by the University of Texas at Austin (UT). The project objective is to gain insight into the nature, formation, occurrence and physical properties of methane hydrate-bearing sediments for the purpose of methane hydrate resource appraisal through the planning and execution of drilling, coring, logging, testing and analytical activities that assess the geologic occurrence, regional context, and characteristics of marine methane hydrate deposits in the Gulf of Mexico outer continental shelf (OCS).

We summarize significant achievements during Phase 4 below.

UT-GOM2-1

1. **AAPG Volume 1 Publication:** A dedicated American Association of Petroleum Geologists Bulletin volume describing the initial results from the 2017 UT-GOM2-1 expedition was published in September 2020. Six papers summarize the initial results of the expedition. This is part 1 of a multi-volume commitment by AAPG to this project. (Section 4.1)
   AAPG Bulletin, Vol. 104, No. 9, *Gas Hydrates in Green Canyon 955, Deep-water Gulf of Mexico: Part 1*
   - http://dx.doi.org/10.1306/01062019165
   - http://dx.doi.org/10.1306/05212019052
   - http://dx.doi.org/10.1306/05212019027
   - http://dx.doi.org/10.1306/01062018280
   - http://dx.doi.org/10.1306/10151818125
   - http://dx.doi.org/10.1306/04251918177
   - http://dx.doi.org/10.1306/02262019036
2. Continued Pressure and Depressurized GOM2-1 Core Analysis:
   - We further confirmed that the natural gas in hydrate at GC-955 was formed by primary microbial processes (>76.1 %) (Section 3.2).
   - The in-situ effective permeability hydrate-bearing sandy silts at the GC-955 reservoir ranges from 0.1 md (1.0×10^{-16} m^2) to 2.4 md ($2.4\times10^{-15}m^2$) in cores with 83% to 93% hydrate saturation. The intrinsic permeability (the single-phase permeability) is estimated from reconstituted samples to be ~12 md (1.2×10^{-14} m^2) to ~41 md (4.1×10^{-14} m^2) (Section 3.2)
   - We used observation and models to interpret that the core degradation that is found in pressure cores is due to dissociation of the methane hydrate in the outer circumference of the core and dissolution of that methane into the fresh pore water that the core is stored with. We are designing approaches to minimize this core loss in the future (Section 3.2).
3. **Pressure Coring Technology Advancement:** We spent an enormous amount of effort to further improve the ability of the pressure coring tool (the PCTB) to pressure seal correctly.
   - **Upper Section Modification:** We completed upgrading the upper section of the PCTB to address poor pressure (Section 3.6.1).

- **Bench Test Upper Section:** We successful tested the modifications at Geotek's test facility in Salt Lake City (Bench Test II) (Section 3.6.2).
- **PCTB Land Test:** We completed a Land Test of the PCTB at the Schlumberger Cameron Test and Training Facility (CTTF). The tool did not seal in 6 out of 7 tests, and we clearly demonstrated that cuttings were wedging in the ball valve assembly, keeping the ball valve from sealing (Section 3.6.3).
- **Further PCTB Testing & Modifications:** We reproduced the failure mechanism observed during the land test at Salt Lake City and confirmed the sensitivity of the ball valve assembly to grit. Geotek designed and tested 9 modifications to address this issue and the PCTB is now 100% successfully sealing in the presence of grit. (See Section 3.6.4).

4. **Preparation for UT-GOM2-2.** Our science expedition is scheduled for spring 2022 and we are fully focused on preparing for this.
    - **Shallow Hazard Assessment:** UT and Ohio State completed a Shallow Hazard Assessment report for each proposed UT-GOM2-2 drilling location, pursuant to 30 CFR 250.214(f) and 250.244 (f). The Shallow Hazard Reports will accompany the UT-GOM2-2 Exploration Plan that is submitted to BOEM, and completes the geological and geophysical analysis for UT-GOM2-2 permitting efforts (See Section 3.7.1)
    - **Operations Plan:** We updated the UT-GOM2-2 Operations Plan (Version 1). We completed the UT-GOM2-2 Science and Sample Distribution Plan (Version 1) (See Section 3.3)
    - **Vessel Selection:** We evaluated the scope, budget, and schedule that would result from using a commercial vessel. We developed detailed drilling schedule, mud volume, and resource estimates. We developed a vessel specification document and a well plan, and sent these documents to prospective vessel contractors. (See Section 3.4)

2 INTRODUCTION

The objective of this project is to gain insight into the nature, formation, occurrence and physical properties of methane hydrate-bearing sediments for the purpose of methane hydrate resource appraisal through the planning and execution of drilling, coring, logging, testing and analytical activities that assess the geologic occurrence, regional context, and characteristics of marine methane hydrate deposits in the Gulf of Mexico Continental Shelf.

The project is being executed in 5 project phases, which correspond to 5 budget periods.

Phase 1 took place between Oct. 1, 2014 and Sep. 30, 2015. In Phase 1, potential UT-GOM2-2 field sites were identified, appraised using available geophysical and geologic data, and ranked relative to one another using criteria developed in conjunction with DOE (TASK 2). Following site selection, a pre-expedition drilling, coring, logging and sampling operational plan was developed (TASK 3). A Complementary Project Proposal (CPP), based on the Operational Plan, was submitted to the International Ocean Discovery Program (IODP) as a primary method of accessing a suitable scientific drilling vessel (TASK 4). Concurrently, lab testing and modification of the pressure coring tool with ball-valve (PCTB) was conducted (TASK 5).

Phase 2 took place between Oct. 1, 2015 and Jan. 15, 2018. In Phase 2, UT continued support of the CPP, and modified the proposal as needed (TASK 6). A land-based field test (Land Test) of the PCTB was conducted (TASK 7). A Marine Field Test (UT-GOM2-1) of the PCTB was conducted, during which hydrate-bearing pressure cores were acquired from two drill-sites in Green Canyon Block 955 in the Gulf of Mexico, outer continental shelf (TASK 8). UT developed the capability to transport, store, and manipulate pressure cores, acquired during the UT-GOM2-1 Marine Field Test (TASK 9). Pressure cores acquired during the UT-GOM2-1 Marine Field Test were transported to land-based facilities, stored, subsampled, and characterized (TASK 10). The Operational Plan for the UT-GOM2-2 Scientific Drilling Program was refined (TASK 11). UT continued to support efforts to acquire access to a scientific drilling vessel, provided updates of CPP outcomes and, evaluated alternate means of gaining access to a vessel for the UT-GOM2-2 Scientific Drilling Program (TASK 12).

Phase 3 took place between Jan. 16, 2018 and Sep. 30, 2019. In Phase 3, UT continued support of the CPP, and modified the proposal as needed (TASK 6). A land-based field test (Land Test) of the PCTB was conducted (TASK 7). A Marine Field Test (UT-GOM2-1) of the PCTB was conducted, during which hydrate-bearing pressure cores were acquired from two drill-sites in Green Canyon Block 955 in the Gulf of Mexico, outer continental shelf (TASK 8). UT developed the capability to transport, store, and manipulate pressure cores, acquired during the UT-GOM2-1 Marine Field Test (TASK 9). Pressure cores acquired during the UT-GOM2-1 Marine Field Test were transported to land-based facilities, stored, subsampled, and characterized (TASK 10). The Operational Plan for the UT-GOM2-2 Scientific Drilling Program was refined (TASK 11). UT continued to support efforts to acquire access to a scientific drilling vessel, provided updates of CPP outcomes and, evaluated alternate means of gaining access to a vessel for the UT-GOM2-2 Scientific Drilling Program (TASK 12).

Phase 4 took place between Oct. 1, 2019 and Sep. 30, 2020. In Phase 4, UT continued to characterize pressure cores acquired from the UT-GOM2-1 Marine Field Test and strengthened analytical capabilities (Task 10.0: Pressure Core Analysis). The UT-GOM2-2 Scientific Drilling Program Science and Sample Distribution Plan and Operations Plan were refined and updated (Task 11.0: Update Science and Operational Plans for UT-GOM2-2). UT continued to pursue access to a suitable drilling vessel for UT-GOM2-2, and developed vessel requirements and well design information for prospective contractors (Task 12.0: UT-GOM2-2 Scientific Drilling Program

Vessel Access). UT maintained and continued to optimize the capability to transport, store, and manipulate pressure cores (Task 13.0: Maintenance and Refinement of Pressure Core Transport, Storage, and Manipulation Capability). The PCTB was bench tested and upgraded. A Land Test of the PCTB was conducted at the Schlumberger Cameron Test and Training Facility, followed by further bench tests and evaluation of the ball-valve assembly (Task 14.0: Performance Assessment, Modifications, and Testing of PCTB). UT initiated permitting efforts for the UT-GOM2-2 Scientific Drilling Program, and completed the Geology and Geophysics section of the Exploration Plan (Task 15.0: UT-GOM2-2 Scientific Drilling Program Preparations).

3 SUMMARY OF PHASE 4 TASKS

Phase 4 tasks are summarized in Table 3-1.

Table 3-1: Summary of Phase 4 tasks

PHASE 4/BUDGET PERIOD 4	
Tasks continued from previous phases	
Task 1.0	**Project Management and Planning**
Task 10.0	**Core Analysis**
Subtask 10.4	*Continued Pressure Core Analysis (GOM2-1)*
Subtask 10.5	*Continued Hydrate Core-Log-Seismic Synthesis (UT-GOM2-1)*
Subtask 10.6	*Additional Core Analysis Capabilities*
Subtask 10.7	*Hydrate Modeling*
Task 11.0	**Update Science and Operational Plans for UT-GOM2-2 Scientific Drilling Program**
Task 12.0	**UT-GOM2-2 Scientific Drilling Program Vessel Access**
Task 13.0	**Maintenance and Refinement of Pressure Core Transport, Storage, and Manipulation Capability**
Subtask 13.1	*Hydrate Core Manipulator and Cutter Tool*
Subtask 13.2	*Hydrate Core Effective Stress Chamber*
Subtask 13.3	*Hydrate Core Depressurization Chamber*
Subtask 13.4	*Develop Hydrate Core Transport Capability for UT-GOM2-2 Scientific Drilling Program*
Subtask 13.5	*Expansion of Pressure Core Storage Capability for UT-GOM2-2 Scientific Drilling Program*
Subtask 13.6	*Continued Storage of Hydrate Cores from UT-GOM2-1*
Subtask 13.7	*X-ray Computed Tomography*
Subtask 13.8	*Pre-Consolidation System*
Task 14.0	**Performance Assessment, Modifications, and Testing of PCTB**
Subtask 14.1	*PCTB Lab Test*
Subtask 14.2	*PCTB Modifications/Upgrades*
Subtask 14.3	*PCTB Land Test*
Task 15.0	**UT-GOM2-2 Scientific Drilling Program Preparations**
Subtask 15.3	*Permitting for UT-GOM2-2 Scientific Drilling Program*

3.1 Task 1.0: Project Management and Planning

Objectives

The Recipient will continue to execute the project in accordance with the approved PMP covering the entire project period. The recipient will manage and control project activities in accordance with their established processes and procedures to ensure subtasks and tasks are completed within schedule and budget constraints defined by the PMP. This includes tracking and reporting progress and project risks to DOE and other stakeholders. The Recipient will review the project PMP at the initiation of each project phase and update as necessary.

Accomplishments

During GOM2 Phase 4, UT accomplished the following project management and planning tasks:

Assembled team to meet project needs

1. Hired the following positions:
    a. Post-doctoral researcher (Alejandro Ramirez)
    b. Research Associate (Aleksei Portnov)
    c. Research and Engineering/Science Associate (Donnie Brooks)
    d. Graduate Student (Gabriella Varona)

Coordinated the overall scientific progress, administration, and finances of the project

1. Monitored and controlled project cost, scope, and schedule.
2. Reported status updates, identified risks, and change requests to DOE Project Manager.
3. Supported UT-GOM2-1 AAPG editors and GOM2 scientists and staff with communications, organizing meetings, and identifying potential topics and authors.
4. Performed extensive evaluation of scope, budget, and schedule implications for UT-GOM2-2.
5. Continued to develop and update cost frameworks, operational plans, schedules, and scientific objectives for UT-GOM2-2.
6. Transitioned the UT Austin GOM2 Research Team to working remotely in response to SARS-CoV-2 (COVID-19) pandemic. Acquired special exemption from the UT Vice President for Research to continue operation and maintenance of the UT Pressure Core Center, and experimentation on pressure cores.
7. Developed and submitted a proposal for $35MM in stimulus funds to the U.S. House of Representatives Committee on Science, Space, and Technology (SST) to augment committed DOE funds.
8. Developed BP4 to BP5 budget period transition proposal and submitted to DOE on June 30, 2020.

Communicated with project team and sponsors

1. Organized regular meetings, including weekly UT Management updates, Monthly Sponsor updates, PCTB Development Team meetings, UT-GOM2-2 Science and Sample Distribution meetings, UT-GOM2-2 Operational Plan meetings, and UT-GOM2-2 Permit meetings, and UT-GOM2-2 Vessel Procurement meetings

2. Presented at the Methane Hydrate Advisory Committee Meeting on February 26, 2020 in Galveston, TX.
3. Managed SharePoint sites developed to facilitate project team collaboration.
4. Managed archive websites for project deliverables.

Coordinated and supervised subcontractors and service agreements

1. Actively managed all Subawards, subcontractors and service agreements, monitored work products/tasks and schedules, verified that contractual obligations were met, reviewed and approved invoices.
2. Executed service agreement amendment with Geotek Coring Inc. (Geotek) for continued PCTB modifications and testing.
3. Executed service agreement with Schlumberger Technology Corporation (STC) for use of the Cameron Testing and Training Facility (CTTF) during the PCTB Land Test.
4. Amended service agreement with Pettigrew Engineering, PLLC (Pettigrew Engineering) for continued engineering and consulting services throughout Phase 4.
5. Amended contract agreement with Ohio State sub-award with new foreign national clause and additional funding for BP5. Ohio State act as the Site Characterization Technical and Science Lead for UT-GOM2-2 and will perform conventional core and gas geochemical analysis.
6. Amended contract agreement with the University of New Hampshire (UNH) with new foreign national clause and additional funding for BP5. UNH will lead the lithostratigraphy effort for UT-GOM2-2.
7. Amended contract agreement with Lamont-Doherty Earth Observatory (LDEO) at Columbia University sub-award with new foreign national clause and additional funding for BP5. Lamont-Doherty will contribute to ensuring that the sampling and analytical plan is appropriate to fully address the expedition objectives, particularly in regard to the physical properties and geochemical observations needed to assess the relative contribution of in situ and migrating methane, long-range aqueous methane migration, and the temporal evolution of hydrate accumulations.
8. Amended contract agreement with Oregon State sub-award with new foreign national clause and additional funding for BP5. Oregon State University will lead the microbiology effort for UT-GOM2-2.
9. Amended contract agreement with the University of Washington (UW) sub-award with new foreign national clause and additional funding for BP5. UW will lead the geochemistry effort for UT-GOM2-2.
10. Finalized a research agreement with AIST (Japan) so that they could work in the pressure core center and safely remove and transfer UT-GOM2-1 pressure core back to AIST for research in their labs using PNATS and other tools.

Identified, monitored, and managed risks, and communicated risks to stakeholders.

1. Actively monitored project risks and reported as needed to project team and stakeholders.
2. The PCTB did not perform satisfactorily during the PCTB Land Test in March, 2020. UT acquired approval from DOE to use savings achieved in BP4 to improve ball-valve performance in BP5.

3.2 Task 10.0: Pressure Core Analysis

3.2.1 Subtask 10.4: Continued Pressure Core Analysis (UT-GOM2-1)

Objectives

The Recipient will continue to perform, or facilitate performance by others, analysis on the hydrate pressure core acquired from the UT-GOM2-1 Marine Field Test in Phase 2, Task 8.

- *For selected samples, permeability will be measured during depressurization*
- *For selected samples, geotechnical properties (such as compression index and Young's modulus) will be measured during depressurization.*

Accomplishments

3.2.1.1 Pressure Core: Quantitative Degassing, Hydrate Saturation, and Gas Analysis

3.2.1.1.1 Hydrate saturation by lithofacies

The results from 30 quantitative degassing experiments completed at UT on pressure cores from the UT-GOM2-1 expedition were summarized and published in the AAPG special edition on GC 955, Vol 104, Sept 2020. (Phillips et al., 2020)). The hydrate saturation (S_h) is 79% to 93% within sandy silt beds (centimeters to meters in thickness). Sandy silt intervals are interbedded with clayey silt sections that have lower S_h (2%–35%) and lower Vp (1684–2023 m s-1). Clayey silt intervals are composed of thin laminae of silts with high S_h within clay-rich intervals containing little to no hydrate. Degassing of single lithofacies sections revealed higher-resolution variation in S_h than is possible to observe in well logs; however, the average S_h of 64% through the reservoir is similar to well log estimates.

A subset of six degassing experiments performed using very small pressure decrements indicates that the salinity within these samples is close to the average seawater concentration, suggesting that hydrate either formed slowly or formed during a rapid event at least tens of thousands of years before present.

3.2.1.1.2 Gas Collection Techniques

UT, with The Ohio State University (Ohio State), continue testing and improving methods of collecting gas samples during quantitative degassing.

UT performed three quantitative degassing experiments (H002-04CS-2, H005-07FB-3, 49-66 cm and H005-2FB2, 5-32 cm). The samples contained multiple lithofacies and were used to collect bulk gas samples for molecular hydrocarbon, bulk methane C and H isotope, and noble gas composition. Gases were collected using an inflatable bag as shown in Figure 3-1.

A methods paper summarizing the improvements in gas collection established by Ohio State and UT was published (Moore et al., 2020). The paper compares data obtained from a commonly used degassing approach to our newly developed modified quantitative degassing (MQD) method designed to minimize atmospheric contamination and gas-water interactions. The old standard method allows sample gas to interact with water in a bubbling chamber altering the gas composition. The MQD method displayed significantly lower concentrations of atmospheric gases, higher proportions of hydrocarbon gases, lower ratios of C1/C2+, and heavier stable carbon and hydrogen isotopes of methane than the standard method, demonstrating that the MQD method reduces air contamination and minimizes alteration of the hydrocarbon composition.

Figure 3-1: Image of inflatable bag attached to the quantitative degassing manifold used in order to capture 100% of the gas produced from the dissociation of hydrate-bearing sediment from UT-GOM2-1. Samples taken from the bag will be used to measure the bulk chemical ratios of the dissociated gases.

3.2.1.1.3 Gas Composition and Interpretation

Gas recovered from the hydrates during the experiments discussed above is composed almost entirely of methane (99.99% CH_4, <100 ppm C_2H_6 on average), with an isotopic composition (δ13C: -60.4% and -63.6% Vienna Peedee belemnite and δ2H: -178.2% and -179.0% Vienna standard mean ocean water, see Figure 3-2 A and B as shown by the white diamonds and red circles), suggesting that the natural gas dissociated from GC 955 hydrates is primarily from a microbial source (Phillips et al., 2020).

Natural gas formed by thermogenic processes is most easily distinguished from microbial sources by the presence of ethane and heavier aliphatic hydrocarbons ([C_2+]) (Jackson et al., 2013) and the C_1/C_2+ of oil-associated natural gas can be as low as 0.1 and increases up to ~100 as gas thermal maturity increases (Bernard et al., 1976), Figure 3-2 A lower red box. Alternatively, regardless of the specific pathway, methanogens produce almost exclusively methane, leading to high C_1/C_2+ (up to 1 x 10^4 for CO_2 reduction or 2 x 10^3 for acetate fermentation) and isotopically-light $\delta^{13}C$ signatures of methane (Bernard et al., 1976) (Etiope, 2017) (Milkov, 2011) (Whiticar et al., 1986), see Figure 3-2 upper blue and black boxes. Increasing thermal maturity also leads to a progressive increase in the stable isotopic composition of carbon and hydrogen in methane and heavier hydrocarbons (Figure 3-2). The $\delta^{13}C$-CH_4 and $\delta^{2}H$-CH_4 of immature oil-associated natural gas is initially approximately -55‰ and -300‰, respectively (Figure 3-3). As temperature increases, the stable isotopic values

of carbon and hydrogen continue to increase and can range up to $\delta^{13}C\text{-}CH_4$ ~ -25‰ and $\delta^{2}H\text{-}CH_4$ ~ -160‰ in post-mature natural gas (Schoell, 1980).

Mixing models (black and grey lines in Figure 3-4) can be used to determine the proportion of microbial or thermogenic natural gas contained within hydrates. Below are the two formulas used to determine the proportion of microbial gas present in our system (Jenden et al., 1993):

Eq. 1. $(C_1/C_2+)_{Mixture} = ((f_{Mic}*[CH_4]_{Mic} + (1-f_{Mic}) * [CH_4]_{Therm})) / ((f_{Mic} * [C_2+]_{Mic} + (1-f_{Mic}) * [C_2+]_{Therm})$

Eq. 2. $(\delta^{13}C\text{-}CH_4)_{Mixture} = ((f_{Mic}*[CH_4]_{Mic}*(\delta^{13}C\text{-}CH_4)_{Mic}) + ((1- f_{Mic}) * [CH_4]_{Therm}* (\delta^{13}C\text{-}CH_4)_{Therm})) / (f_{Mic}*[CH_4]_{Mic} + (1-f_{Mic}) * [CH_4]_{Therm})$

Where, f_{Mic} is the proportion of microbial gas in the mixture and $[CH_4]_{Mic}$, $[C_2+]_{Mic}$ and $(\delta^{13}C\text{-}CH_4)_{Mic}$ represent the methane and ethane concentrations and carbon isotopic composition of the microbial endmember, respectively. The $[CH_4]_{Therm}$, $[C_2+]_{Therm}$, and $(\delta^{13}C\text{-}CH_4)_{Therm}$) represent the methane and ethane concentrations and carbon isotopic composition of the thermogenic endmember, respectively.

Based upon the three figures below and the two equations above, we can determine that natural gas was formed predominantly by primary microbial processes (>76.1 %). This is determined by using a hydrogenotrophic methanogenesis endmember ($d^{13}C\text{-}CH_4$= -75‰ and C_1/C_2+= 10,000) and the previously published geochemical data (Sassen et al., 2003) from the underlying Genesis oil and gas field ($d^{13}C\text{-}CH_4$= -55.3‰ and C_1/C_2+= 10.7).

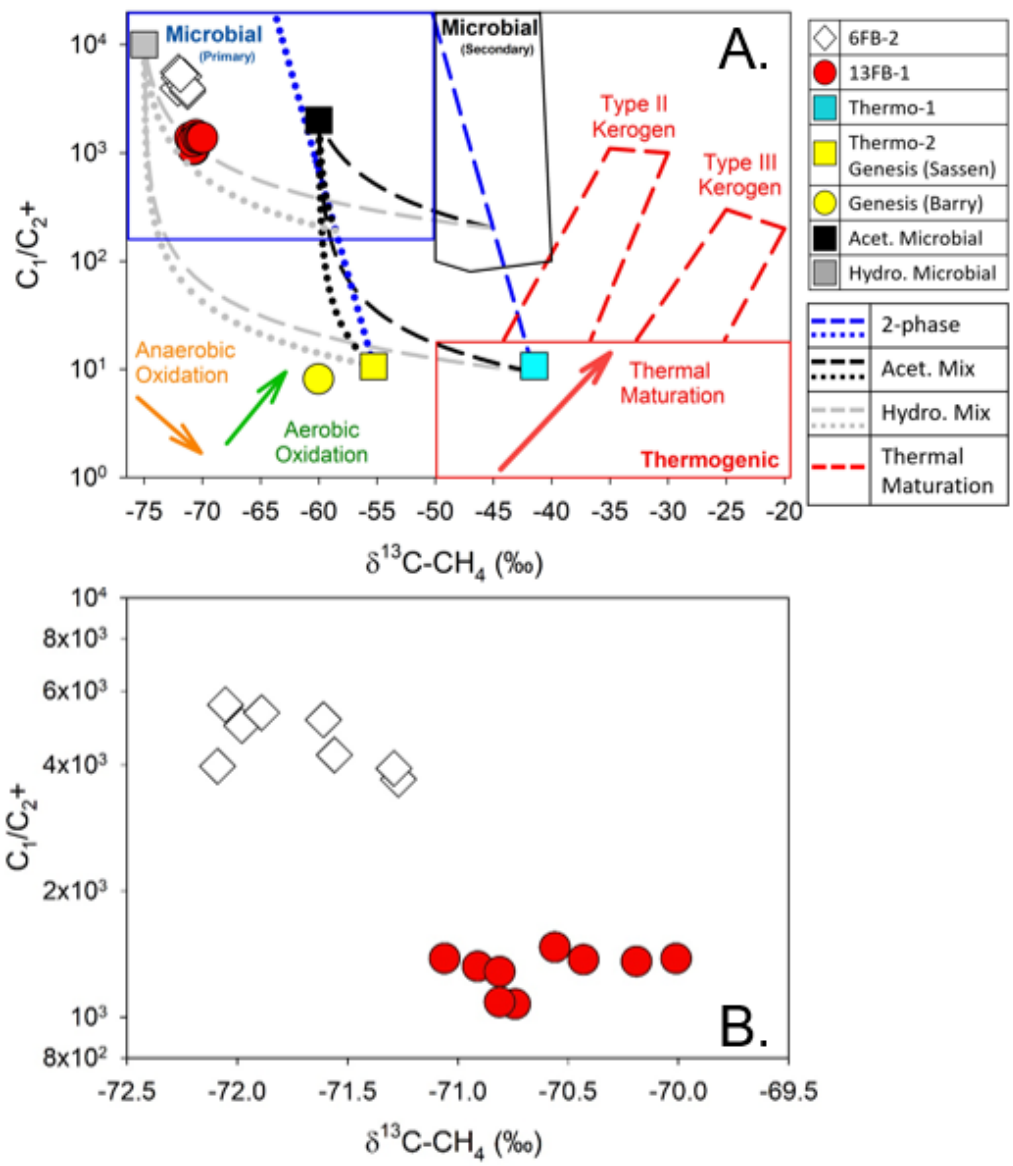

Figure 3-2: Scatter plots of C_1/C_2+ versus $\delta^{13}C\text{-}CH_4$ (top, A) and a zoomed in plot of just UT-GOM2-1 samples (bottom, B). A. Measured gas samples collected in the present study are shown in the upper left (white diamonds for section 6FB-2 and red circles for section 13FB-1) and are compared to samples from previously published data from the Genesis Oil and Gas Field (yellow square, (Sassen et al., 2003); yellow circle,(Barry et al., 2018). The blue box represents the ranges of typical primary microbial methane generation. The black box represents secondary microbial methane. The red box represents thermogenic methane and the red arrow and dashed boxes are the trends of thermogenic natural gas maturation based on a Type II or Type III kerogen source rock (Schoell, 1980) (Bernard et al., 1976) (Milkov and Etiope, 2018). Paths of possible post-genetic modification of Thermo-1 (calculated based on R_o,) (McBride et al., 1998) (Schoell, 1983) start at the cyan square and move along the dashed lines. Paths of possible post-genetic modification of Thermo-2 (Genesis gas) start at the yellow square and move along the dotted lines. Modification from 2-phase solubility fractionation is shown in blue (Darrah et al., 2015) (Harkness et al., 2017) (Moore et al., 2018). Modification from thermogenic endmembers mixing with hydrogenotrophic is shown in the lower grey lines. Acetoclastic biogenic modification endmembers are shown in the lower black lines (Jenden et al., 1993). Modification by mixing between migrated thermogenic natural gas that already experienced some post-genetic fractionation and biogenic methane endmembers is represented by the upper black and grey lines. Trends for aerobic oxidation and anaerobic oxidation of methane are shown for comparison by the green arrow and orange arrow, respectively. B. A zoomed-in view of the measured gas samples collected in the present study (white diamonds for section 6FB-2 and red circles for section 13FB-1).

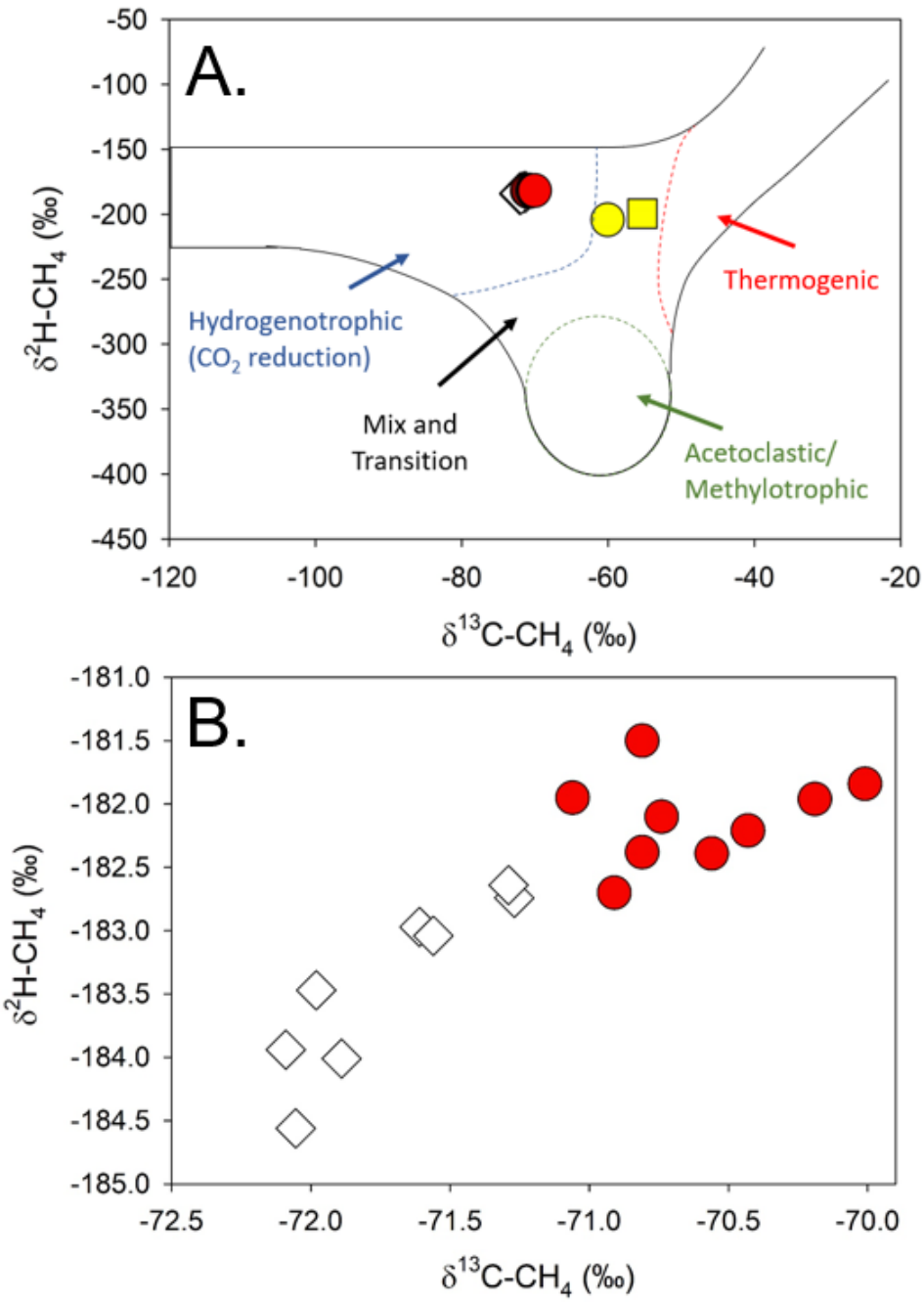

Figure 3-3: Scatter plot of δ^2H-CH_4 vs. δ^{13}C-CH_4 (top, A) and zoomed in (bottom, B) showing data from the present study (white diamonds for section 6FB-2 and red circles for section 13FB-1) in comparison to previously published data from the Genesis Oil and Gas Field (yellow box,(Sassen et al., 2003);and yellow circle, (Barry et al., 2018). In Figure 3-4A, zones for methane formed by hydrogenotrophic (blue) and acetoclastic (green) methanogenesis, thermogenic (red) natural gas are shown for comparison (Vinson et al., 2017).

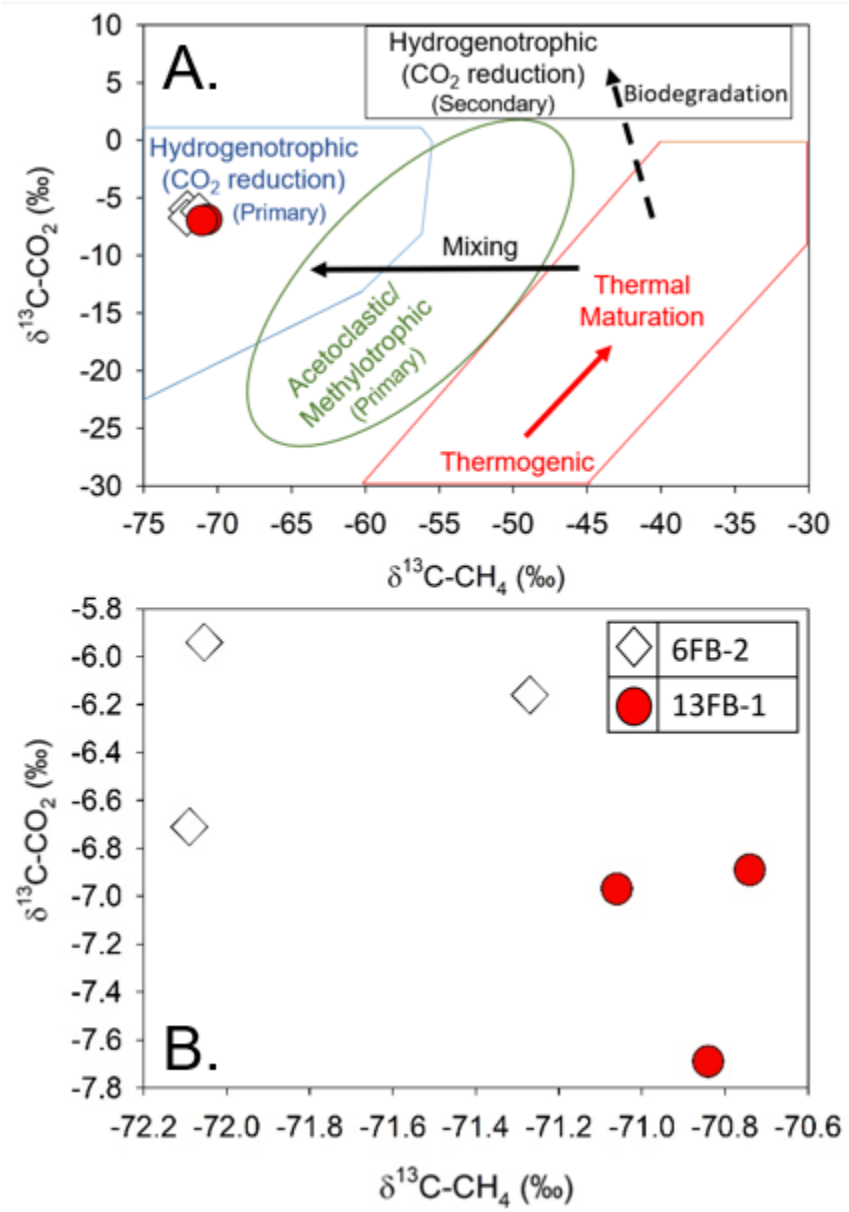

Figure 3-4: Scatter plot of δ^{13}C-CO_2 vs. δ^{13}C-CH_4 (top, A) and zoomed in (bottom, B) showing data from the present study (white diamonds for section 6FB-2 and red circles for section 13FB-1). In Figure A, zones for methane formed by primary hydrogenotrophic (blue) and acetoclastic (green) methanogenesis, secondary hydrogenotrophic methanogenesis (black), thermogenic (red) natural gas are shown for comparison along with trends for mixing (black arrow), thermal maturation (red arrow), and biodegradation of hydrocarbons (black dashed arrow) (endmembers reproduced from (Milkov, 2011; Milkov and Etiope, 2018).

3.2.1.2 Pressure Core: Permeability

3.2.1.2.1 Steady-State Permeability Tests

UT continued measuring the permeability of UT-GOM2-1 hydrate-bearing pressure cores. We successfully measured the effective permeability of four 7FB-3 cores (7FB-3-01, and -03, -04) and one 2FB-2 core (2FB-2-01) with brine and compared the results to previous measurements from 4FB-8 and 13FB-1 (Figure 3-5). We found that the effective permeability (about 23 mD) of 7FB-3-04 (Figure 3-5 dark yellow stars) is much higher than the

values of other 7FB-3 samples. However, this high effective permeability may not be accurate because the sample is highly fractured and also embedded with a small piece of core liner (Figure 3-6, see the light sharp shape in sub figure d). We found that the effective permeability of core 2FB-2-01 (Figure 3-5 green circles) does not decrease with increasing effective stress like the other samples. At in situ stress, the effective permeability is about 2 mD for 2FB-2-01.

We also measured the effective permeability of 7FB-3-03 core with freshwater to examine the effect of clay swelling on the permeability result. We found that the effective permeability did not decrease as expect with clay swelling. Instead, the effective permeability under freshwater increased about 2 mD. This permeability increase is possibly caused by the dissolution of hydrate in freshwater that was injected to displace the brine.

Two manuscripts covering this work are being prepared by UT and will be submitted to AAPG in Phase 5. The first paper presents a comprehensive analysis of permeabilities of hydrate-bearing sandy silt (Fang et al., Submitted-b). The second paper explores in-situ porosity, compressibility, stress state, and frictional strength (Fang et al., Submitted-a). If accepted, these papers will appear in the 2nd AAPG Special volume on GC 955 (Vol 2).

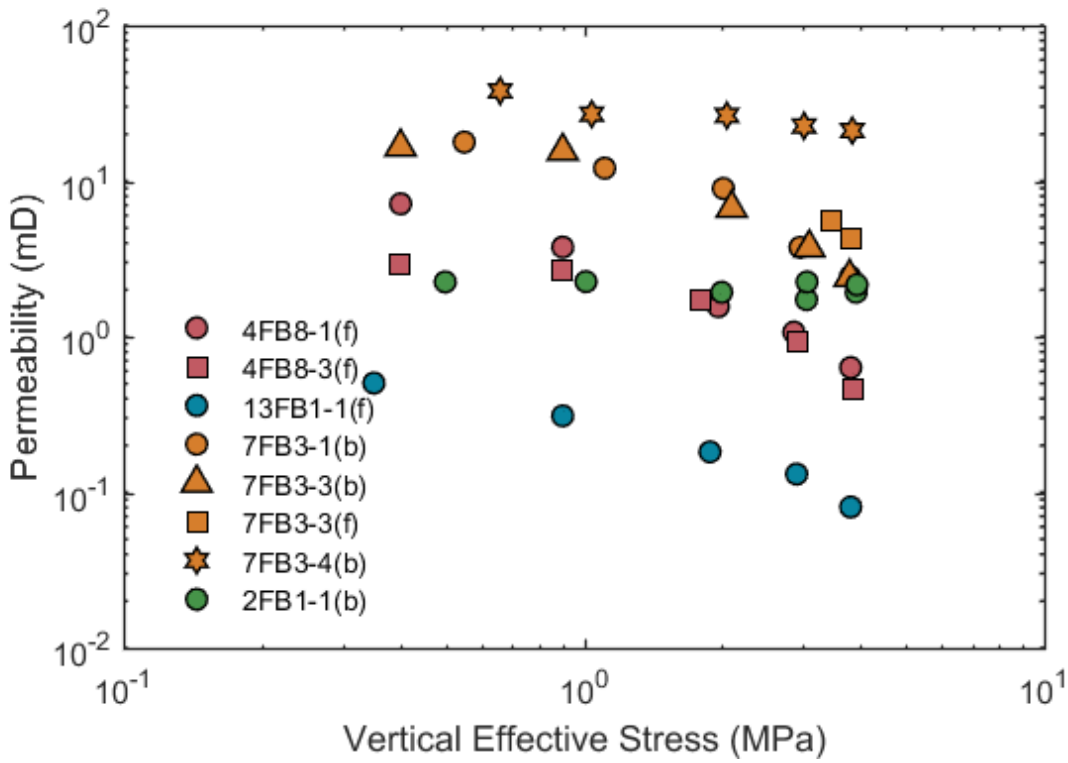

Figure 3-5: A summary of effective permeabilities of UT-GOM2-1 hydrate bearing sandy silt sediment from pressure core sections as a function of vertical effective stress. Legend note: b-measured by brine (salinity = 3.5%), f-measured by freshwater (salinity = 0). During the test, the pore fluid pressure is 24.8 MPa and temperature is 6.5 °C.

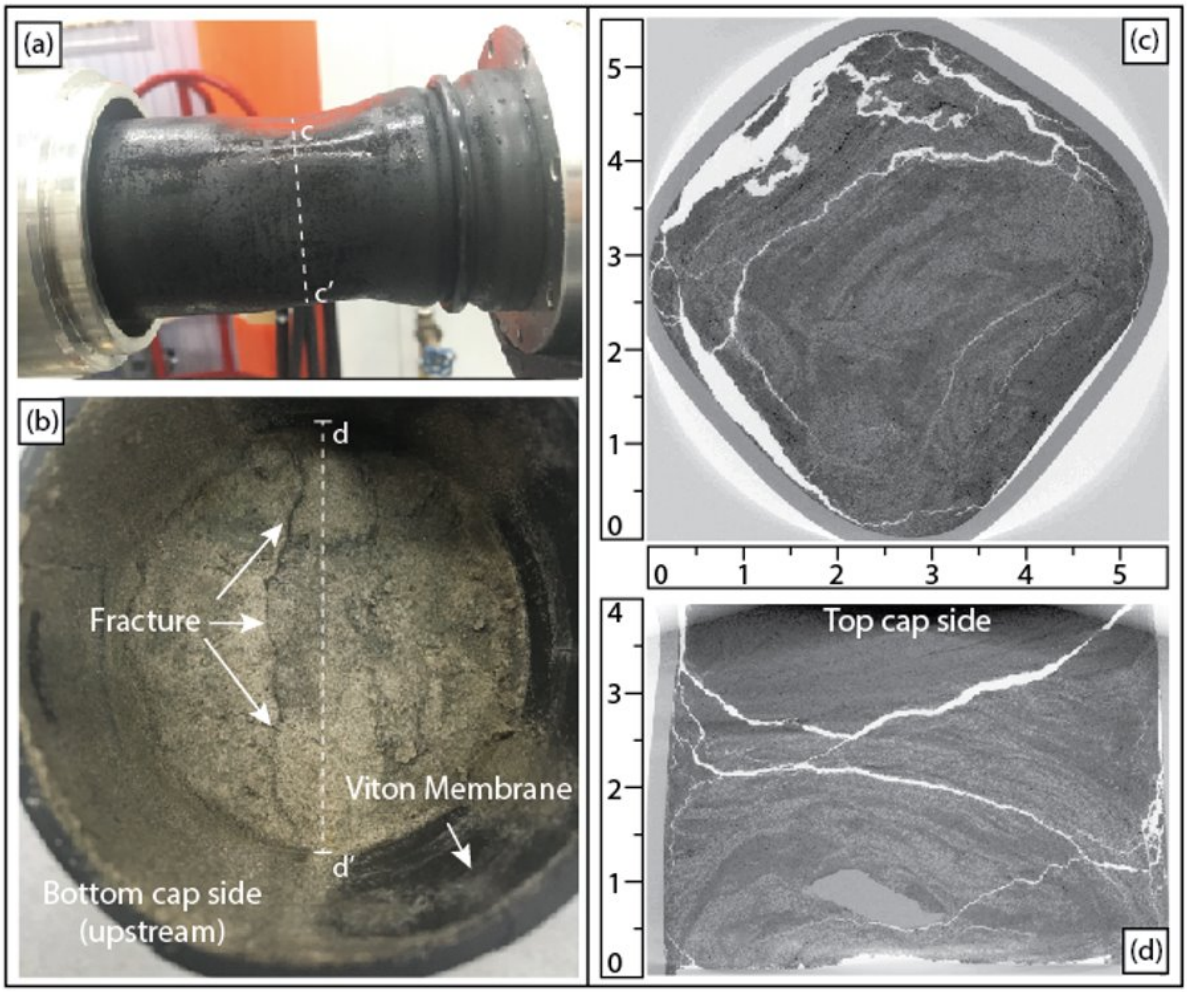

Figure 3-6: Photo and CT image of core 7FB3-04 after hydrate dissociation. (a) Core sample in the core membrane after disassemble the core holder. (b) The bottom cap side of the sample with a fracture trace. (c) The CT-image cross-section view of (c-c') in (a). (d) The CT-image cross-section view of (d-d') in (b).

3.2.1.2.2 Depressurized Core: Intrinsic Permeability of GC 995 Lithofacies through Reconstitution

A paper summarizing the Phase 3 and Phase 4 reconstitution work was published (Fang et al., 2020). Sandy silts reconstituted to the in-situ porosity have a permeability of 11.8 mD ($1.18\times10^{-14}m^2$). Reconstituted clayey silts have a much lower intrinsic permeability of 3.84×10^{-4} mD (3.84×10^{-19} m^2) at the in-situ stress. Reservoir properties were upscaled from these values to estimate the behavior of interbedded sandy silt and clayey silt (Fang et al., 2020). The upscaled intrinsic horizontal and vertical permeabilities for the entire reservoir interval are 8.6 mD (8.6×10^{-15} m^2) and 1.4×10^{-3} mD (1.4×10^{-18} m2). We estimate that during reservoir production, a maximum vertical strain of approximately 12% will result. One additional sample of UT-GOM2-1 material was reconstituted from 7FB-3 sediments during Phase 4 using the under-compaction technique described in Fang et al. (2020). We measured its intrinsic permeability (~41 mD) at porosity of 40%. Figure 3-7 shows a comparison of the results with previous results from Phase 3 on 4FB-8 and 13FB-1.

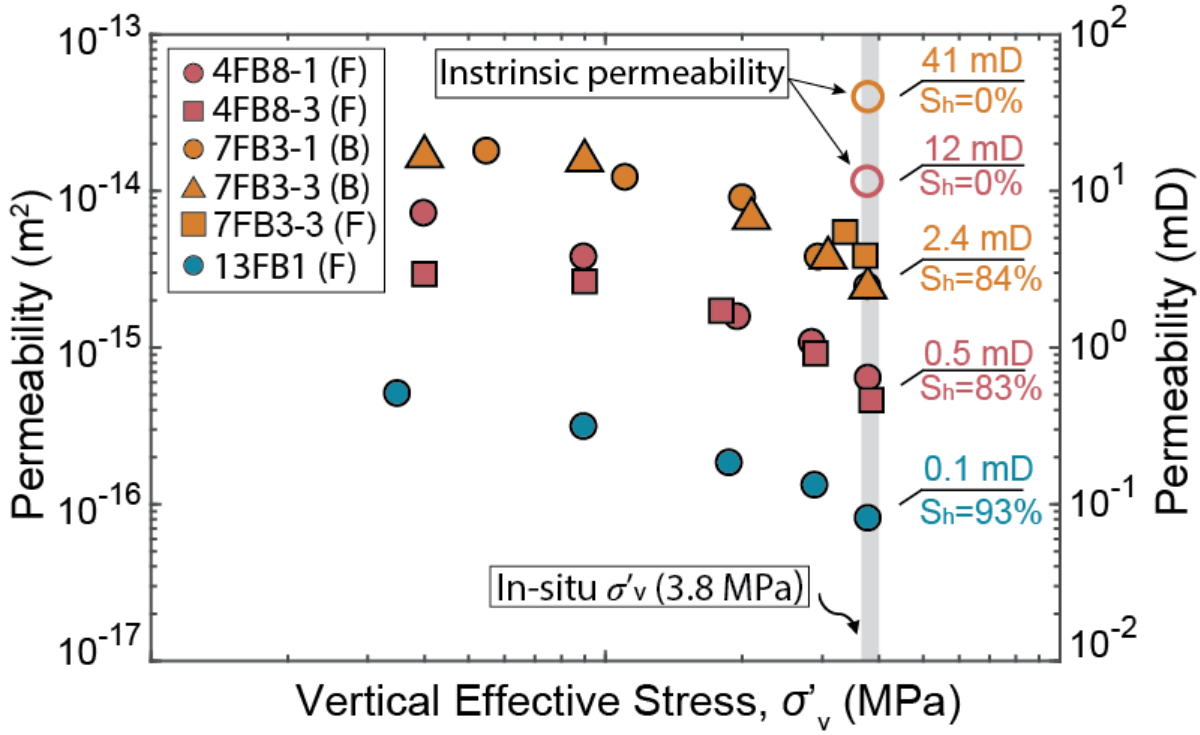

Figure 3-7: Permeability of UT-GOM2-1 Sandy silt sediment from three pressure core sections as a function of vertical effective stress before (effective permeability). The intrinsic permeability is measured by reconstitution approach. B-brine (3.5% salinity), F-freshwater.

3.2.1.3 Pressure Core: Micro-Raman measurements of hydrate cage structure

Micro-Raman spectroscopy scans of hydrate bearing material under pressure were taken at UT by Professor Lin. A section of pressure core H005-07FB-3 was cut and moved into the micro-Raman high pressure analysis chamber. The chamber was taken out of the cold lab and tilted slightly to allow the sediment to rest right against the chamber sapphire window and Raman scans were taken using a Horiba micro-Raman spectrometer. Raman spectroscopy measures the vibrations and rotations of molecules and can distinguish between free methane molecules and molecules trapped in large or small hydrate cages. Intensity of the Raman spectrum at a given point and wavelength shift is proportional to the local concentration of molecules at that point. Figure 3-8 A shows an image of the Horiba micro-Raman system from Professor Lin's lab in the UT Pressure Core center with the micro-Raman chamber in the background. Figure 3-8 B shows images of the UT-GOM2-1 sediment against the sapphire glass and a photo of the micro-Raman lens next to the sapphire glass during scanning using a blue laser (wavelength 473 nm). Exxon Mobil provided funding for the development of the micro-Raman system and high pressure analysis chamber. Figure 3-9 shows two-dimensional Raman maps and cage ratio results from the first scans of a pressure core from the Gulf of Mexico. Figure 3-9(a) shows the relative positions of testing areas on the sample compared to the full sapphire window. Figure 3-9(b) Mapping results of area 1. (c) Mapping results of area 2. The upper panels in Figure 3-9(b) and Figure 3-9(c) are maps of the ratio of the quantity of methane in large cages (peak Raman shift at 2903 cm-1) versus that of small cages (peak Raman shift at ~2905 cm-1). The ratios were calculated from the ratio of the peak area of the large cage over that of the small cage. The lower panels in (b) and (c) show the peak area of large cages as a function of that of small cages

for each measurement with the area normalized to the maximum peak area of large cages. The ratio of large to small cages is indicative of the hydrate structure, sI or sII.

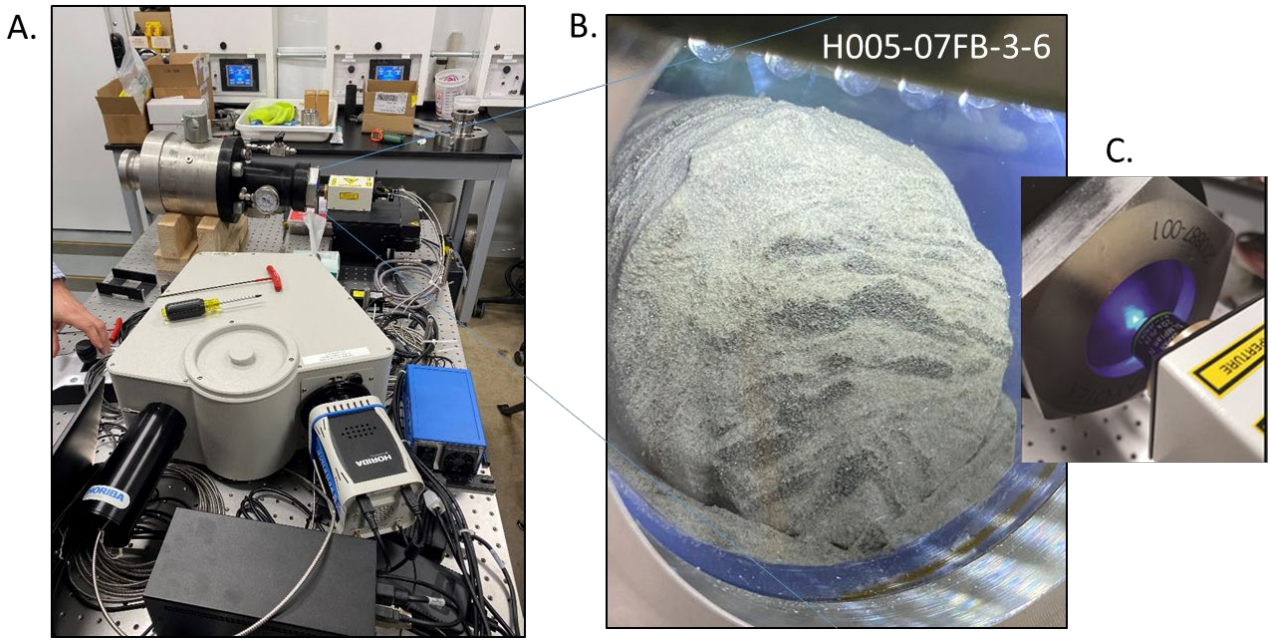

Figure 3-8: micro-Raman spectrometer set up in the UT Pressure Core Center A. micro-Raman Pressure chamber connected to a Horiba Raman system (Lin). B.Hydrate-bearing sediment as seen through sapphire window of micro-Raman Pressure chamber. C. Photo of the Horiba Raman system lens next to the sapphire window during imaging using a blue laser (wavelength 473 nm).

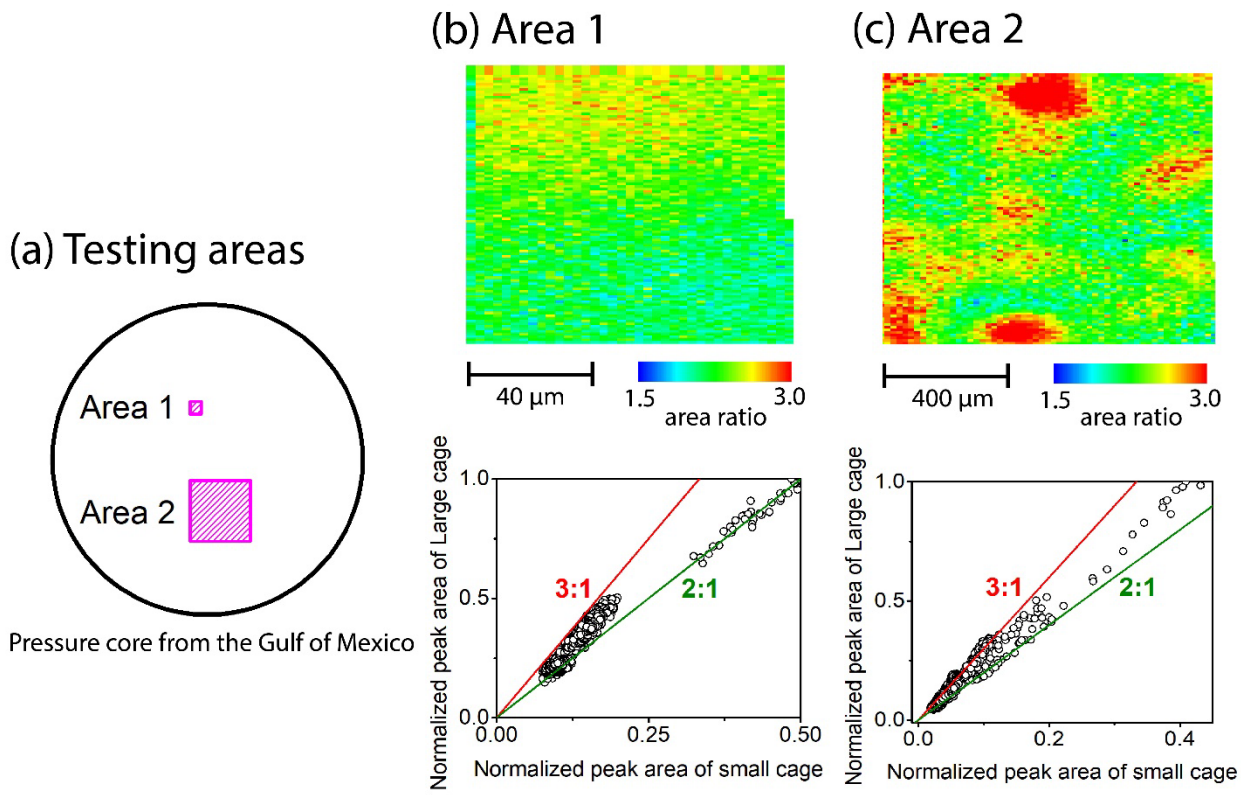

Figure 3-9: Two-dimensional Raman maps of a pressure core from the Gulf of Mexico. (a) Relative positions of testing areas on the sample. (b) Mapping results of area 1. (c) Mapping results of area 2The upper panels in (b) and (c) are maps of the ratio between the quantity of large cages and that of small cages, which were calculated via peak area of large cage over that of small cage. The lower panels in (b) and (c) show the peak area of large cages as a function of that of small cages for each measurement with the area normalized to the maximum peak area of large cages. Two lines represent 3:1 and 2:1 area ratios are plotted in red and green, respectively. The ratio of large to small cages is indicative of the hydrate structure, sI or sII. sI is the more thermodynamically stable structure and has a large to small cage ratio of 3:1.

3.2.1.4 Pressure Core: Assessing Core Degradation during long-term storage

An initial technical assessment of the degradation of pressure cores from UT-GOM2-1 during long term storage was started in order to determine any actions that might be taken prior to UT-GOM2-2 in order to better preserve the core.

Pressure cores are stored inside high pressure storage chambers with fresh water surrounding the core liner. Core degradation is assumed to result from methane dissociating from hydrate within the core and dissolving into the fresh water over long periods of time. We calculated the amount of methane that could dissolve into the storage water assuming no methane was present initially. The methane mass balance calculation assumed the core had 40% porosity, 90% hydrate saturation, was 111 cm long, and was composed of homogeneous sandy silt. The total volume of storage fluid with the core was calculated to be 1.3 L. The mass balance estimate predicted that 25 mL of hydrate (1.9% of the hydrate originally in the core) would dissociate and dissolve into the 1.3 L of storage fluid. Radial core loss was estimated from the volume of hydrate lost assuming a homogeneous porosity of 40%, a hydrate saturation of 90%, a perfectly round core, that hydrate is homogeneously lost along the outside of the core, and core sediment falls away from the core as the hydrate

dissociates. Thus, 25 mL of hydrate loss equates to the core radius shrinking by 0.15 mm homogeneously along the entire length of the core.

Figure 3-10 shows an example of the degradation for core H005-05FB-3. Core degradation appears to be higher at the bottom of the core. The cores are stored with their bottoms facing upwards. Thus, the end of the core that is open to the storage fluid and faces upward during storage is most degraded. Core degradation was estimated from the images by comparing the core diameter for four different biscuits before and after storage (Figure 3-10, yellow boxes). The radial loss from each biscuit was determined to be 1.8 mm, 1.8 mm, 0.7 mm, and 0 mm, for biscuits 1 through 4, respectively, with a high margin of error. Using the assumptions above, this core radial loss equates to a hydrate volume loss of 34 mL. Thus, the estimate of the loss using a mass balance approach and from inspection of the core images is within a factor of two. We believe we can account for most of the core loss from exposure to fresh (0% salinity, 0% dissolved methane) storage fluid during longer periods of core storage. Additional work to understand and mitigate core degradation will be done in Phase 5 in preparation for UT-GOM2-2.

Figure 3-10: Images of the bottom 77 cm of core section H005-05FB-3 from before and after storage. Top image: CT 3D) cross section (slab section) of the bottom 77 cm of 5FB-3 taken using PCATS during the expedition in May of 2017. Lower density is light-colored and higher density is dark-colored. Biscuits of interbedded layers of sandy silt and clayey silt are evident. Core outer edge is cleanly cut. The bottom-most biscuit of sandy silt (far left) is slight smaller than higher up the core. Bottom image: X-ray (2D) image of the bottom 77 cm of 5FB-3 taken using Mini-PCATS after 2 years of storage in June of 2019 during which time the storage fluid was fully replaced once. Higher density is light-colored and lower density is dark-colored. The core edge after storage, especially at the very bottom (far left), is uneven and the diameter is reduced. Sediment appears to have fallen away and collected in the water between the core and the core liner. Clayey silt biscuit (#4, far right) appears to have little to no radial loss. Yellow boxes show the biscuits and identified core diameter for each of four biscuits used to estimate core loss.

3.2.1.5 Pressure Core: Sample Distribution

UT completed the transfer of all approved pressure and depressurized cores to all institutions. The final pressure core samples were picked up by Geotek, Ltd and arrived at the National Institute of Advanced Industrial Science and Technology (AIST) (Sapporo, Japan) in Spring 2020.

3.2.1.6 Pressure Core: Collaborations

UT continued hosting a bi-weekly international meeting on the petrophysics of hydrate-bearing sediment called the Petrophysics Working group. Attendees of the meeting include all the parties receiving UT-GOM2-1 pressure core samples. The meeting has become an important venue for refining complex laboratory equipment and experimental designs and for advancing our understanding of the behavior of hydrate-bearing sediment at in situ and other conditions. Our Japanese and USGS colleagues have a vast amount of experimental expertise and

they have shared ideas freely. Many members of the group are refining publications which they plan on submitting to one of the AAPG Special Volumes on GOM GC 955.

UT, Ohio State, University of New Hampshire, Oregon State, Columbia University, and University of Washington all participated in the Gordon Research Seminar and Conference on Gas Hydrates including three invited GRS talks. The GRS presentation titled "Coupled Multiphase Flow and Reactive Transport Processes in Gas Hydrate Systems" by You et al. was one of three selected from GRS for a second presentation at GRC.

AAPG Editors, including UT and Ohio State, and the GC 955 Petrophysics Working group, hosted an on-line and in-person (during GRC 2020) workshop. The workshop reviewed the status of all petrophysical and geomechanical experiments on GC 955 pressure core and the status of all possible AAPG submissions to the AAPG Special Bulletin Volume 2.

3.2.1.7 Depressurized Core Analysis: Microbiology

Oregon State with Texas A&M Corpus Christi (TAMU-CC) and ExxonMobil are continuing to test sediment from UT-GOM2-1 pressure cores de-pressurized at UT to determine the microbial community characteristics in the samples that have been stored since 2017. The microbial community was originally characterized at Exxon Research by Zara Summers and Ian Drake and will be used as a point of comparison for communities derived from the core that was de-pressure in 2019. Initial DNA and RNA extraction trials were unsuccessful. Possible reasons include:

- DNA binding to sediments interfering with extraction efficiency;
- Inhibition of DNA amplification by other materials in the sediments that co-extracted with the DNA;
- Loss of microbial cells that were originally present in the samples (and detected by Drake and Summers) during the 2+ year storage period;
- A combination of the factors noted above

The team confirmed that the samples possess low biomass but were preserved and sampled without notable contamination. A separate consideration of pressure and compaction in fine-grain materials such as would occur in the GOM2-1 samples suggests that cells in the GC955 sediments may face a different survival challenge that just pressure alone. In this case, cells appear to exist in the sediments that are compacted to the extent that some of the cells may be physically crushed or pierced by the close contact with sediment grains that are close to the size of the cells themselves. This concept was described by (Rebata-Landa and Santamarina, 2006) and should be a consideration in our study.

Additional extractions were planned for Phase 4 but could not be completed as the labs were closed for the pandemic and did not reopen in Phase 4.

3.2.1.8 Depressurized Core Analysis: Lithostratigraphy

UNH continued to work on synthesizing the grainsize, CHNS, and sediment composition data to document the sediment transport regimes throughout the reservoir and subsequent early diagenesis of the GC-955 hydrate-bearing sediments. Figure 3-11 shows the sorting of all Bulk and Organic Carbon-Free GOM2-1 samples measured to date plotted against their median grain size by laser diffraction. Smaller sorting values equate to better sorting while smaller Phi values equate to larger grain sizes. The UNH lab standard, Wallis Beach Sand, a natural beach sand, is also shown for reference. Sorting was calculated by the Folk and Ward (1957) sorting equation. All the measurements document a silt dominated reservoir, with three distinct sediment facies defined by their grain size distributions and sorting characteristics: Type C samples are the coarsest samples but

have variable sorting that is consistent with turbidite deposition from variable energy turbidity currents. Type B and Type A samples are finer grained and less sorted, characteristic of fine grained deposition during the waning energy of turbidity currents and lower energy hemipelagic settling between turbidity current events. The increased sorting of all samples after organic carbon removal, reflects the variable size of organic carbon deposited during and between turbidity current events and documents that both the turbidites and intervening clays contain measurable organic carbon. In terms of textural classification, Type A samples range from silty clays to clayey silts, Type B samples are clayey silts, and Type C samples range from silty sand to sandy silt. UNH is preparing a paper for submission to AAPG on the final results.

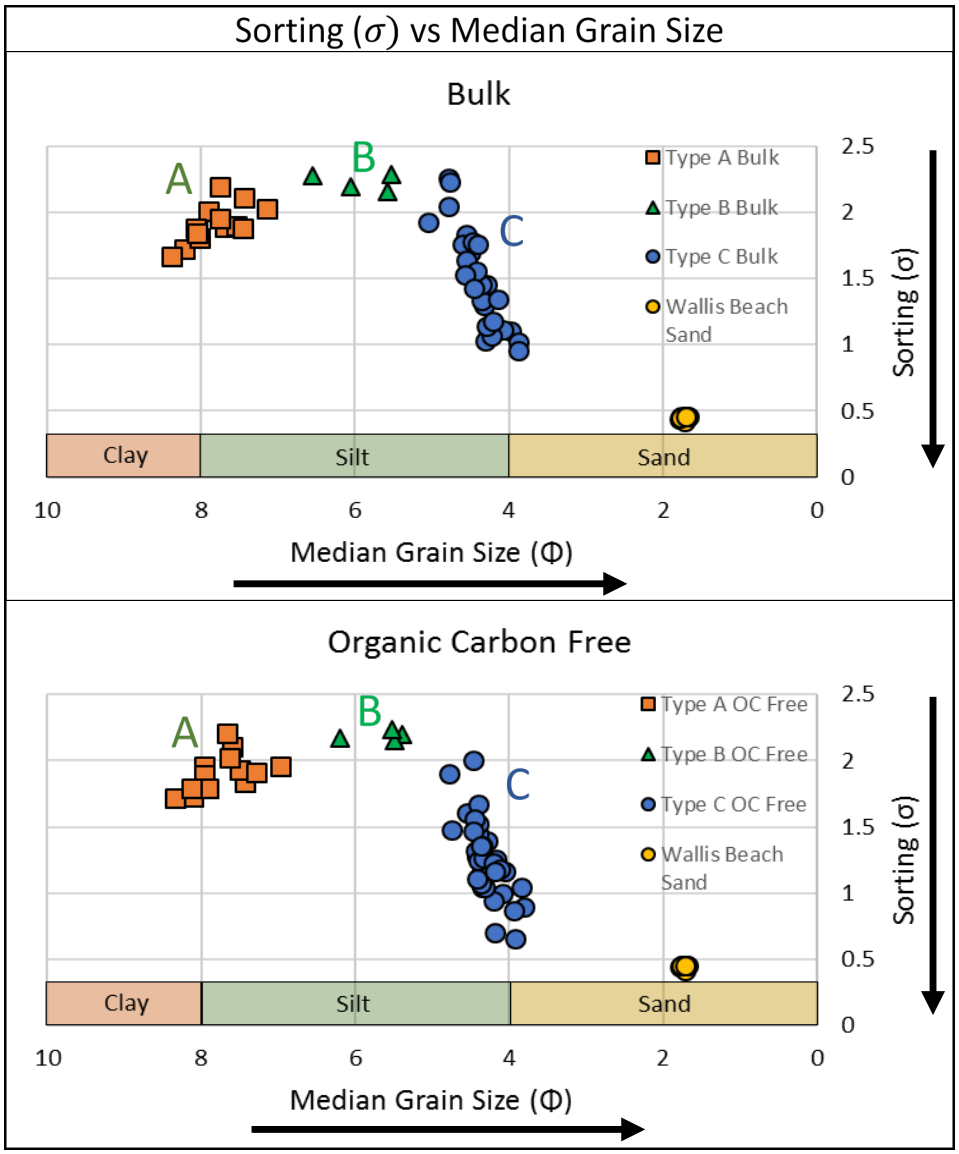

Figure 3-11: Sorting of all Bulk and Organic Carbon-Free GOM2-1 samples plotted against their median grain size (Phi units) from measurements of grain size completed at UNH using laser diffraction. Smaller sorting values equate to better sorting while smaller Phi values equate to larger grain sizes. The UNH lab standard, Wallis Beach Sand, a natural beach sand, is also shown for reference. Sorting was calculated by the Folk and Ward (1957) sorting equation.

3.2.2 Subtask 10.5: Continued Hydrate Core-Log-Seismic Synthesis (UT-GOM2-1)

Objectives

The Recipient will perform, or facilitate performance by others, analysis on the hydrate pressure core data acquired in Phase 2.

- *The measurements of hydrate concentration from Core Analysis will be compared to estimates derived from logging data and anisotropy models of the logging data.*
- *Petrophysical models will be developed to predict the physical and acoustic behavior of the hydrate reservoir as a function of hydrate and pore fluid saturation.*

Accomplishments

No update this period

3.2.2.1 GC 955 Lithofacies Characterization

Work on GC 955 lithofacies characterization was published in the AAPG Special volume on GC 955, Issue 104, 9 (Meazell et al., 2020).

3.2.3 Subtask 10.6: Additional Core Analysis Capabilities

Objectives

The Recipient may develop additional core analysis capabilities including, but not limited to:

- *Mercury porosimetry for both porosity and pore throat analysis.*
- *Scanning Electron Microscope (SEM) for sediment fabric and microstructure.*
- *X-ray Diffraction (XRD) for sediment mineralogy*
- *Grain size analysis using a hydrometer or sieves*
- *Carbon isotopes of organic matter in mud samples.*

Accomplishments

We have developed a suite of analysis approaches to illuminate the material and petrophysical behavior of our cored samples. Additional work on particle size distribution and mercury porosimetry was completed during Phase 4.

3.2.3.1 Particle Size Distribution

52 samples for sediment grain size from holes H002 and H005 using the laser particle size analyzer at UNH were measured twice, (bulk sediment and TOC-free sediment) using the UNH Malvern Mastersizer 2000 Laser Particle Size Analyzer. Three data reports were submitted to UT (on grain size distribution, lithostratigraphy, and biostratigraphy) and a paper summarizing the lithostratigraphy and biostratigraphy of the hydrate-bearing reservoir at GC 955 was started and is being prepared by UNH. (Johnson et al.)

3.2.3.2 Mercury Porosimetry

A paper reviewing the capillary behavior of the (Daigle et al, in press) of the three lithofacies identified at GC 955 was submitted and accepted for the 2nd AAPG Special Volume on GC 955.

3.2.4 Subtask 10.7: Hydrate Modeling

Objectives

Petrophysical models will be developed to predict the flow behavior of sandstone hydrate reservoirs during depressurization and these will be compared to observations on the core.

Accomplishments

Three different thermodynamic hydrate models were developed during Phase 4. The first was a bulk equilibrium model to predict the amount of hydrate dissociation during shut in. The second was a radial 2D numerical model to predict the dissociation behavior in a closed chamber which contains hydrate-bearing core. The third was a similar 2D radial numerical model as the second to describe the loss of hydrate from hydrate-bearing pressure core during long-term storage.

3.2.4.1 Bulk Equilibrium depressurization model

We developed bulk equilibrium-based analytical models to predict the amount of hydrate dissociation during each shut in. In the first case (a to b in Figure 3-12), we assume isothermal and the system is perturbed from point a to point b. In the second case, we consider a condition where hydrate dissociates endothermically but ignore heat flow, the system would return to the phase boundary along the path from b to c (Figure 3-12).

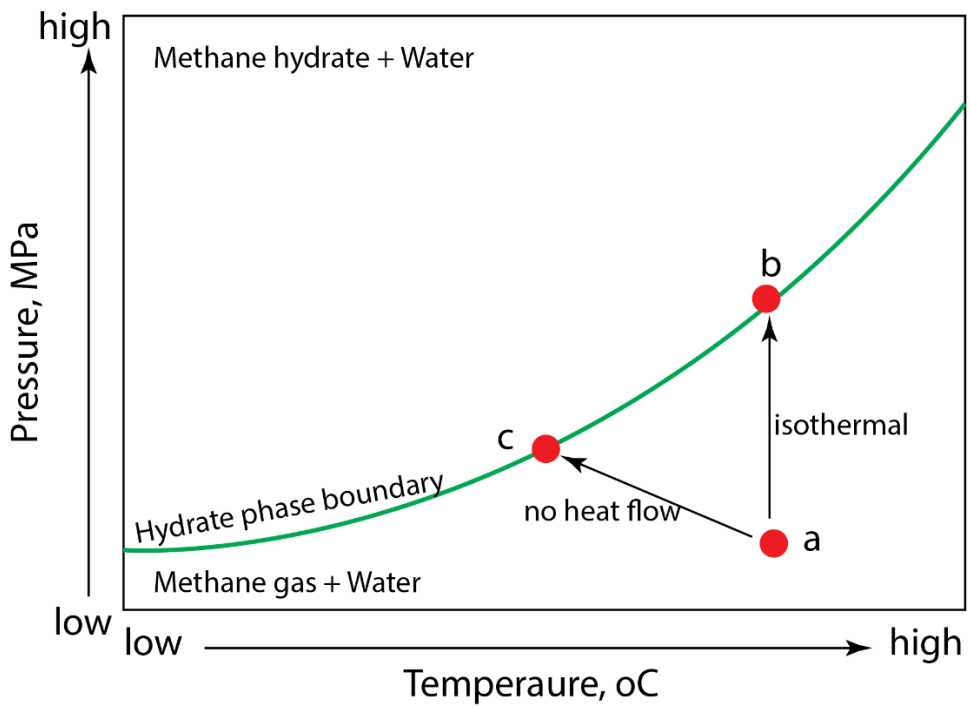

Figure 3-12: Schematic diagram of the response to a pressure perturbation of a hydrate-bearing sample during isothermal dissociation (from point a to point b) and endothermically dissociation without heat flow (from point a to point c) followed by a shut-in interval.

We calculate the volume of hydrate needed to drive the system from a pressure minimum (point a in Figure 3-12) to the hydrate phase boundary along an isothermal pathway (from point a to point b in Figure 3-12) or in a pathway involving no heat flux to the sample (from point a to point c in Figure 3-12), assuming a constant total volume and water with zero compressibility.

The volume of hydrate dissociation (dV_h), as well as the volume of water (dV_w) and volume of methane gas (dV_g) that will be generated, can be calculated as:

$$dV_w = \frac{dV_h \rho_h X_h^w}{\rho_w}, \quad (1)$$

$$dV_g = dV_h - dV_w = \left(1 - \frac{\rho_h X_h^w}{\rho_w}\right) dV_h, \quad (2)$$

Where ρ_h and ρ_w are the density of methane hydrate and water, respectively; X_h^w is the mass fraction of water in methane hydrate.

Isothermal case:

$$\frac{P_b V_b}{n_b z_b} = \frac{P_a V_a}{n_a z_a} \quad (3)$$

where P_a is the gas pressure after hydrate dissociation, which can be calculated from methane hydrate boundary at temperature T_a and the salinity of the system. V_a and V_b are the volumes of methane gas after (point a) and before (point b) hydrate dissociation, respectively, and V_a can be calculated as

$$V_a = V_b + dV_g = V_b + (1 - \frac{P_h X_h^w}{P_w}) dV_h. \quad (4)$$

n_a and n_b are the number of moles of methane in the gas phase after (point a) and before (point b) hydrate dissociation, respectively, and n_a can be calculated as

$$n_a = n_b + dn = n_b + \frac{dV_h P_h X_h^m}{M_m}. (5)$$

z_a and z_b are the gas compressibility after (point a) and before (point b) hydrate dissociation, respectively, which are functions of pressure and temperature.

By substituting of Equations (4) and (5) into Equation (3), and we obtain

$$\frac{P_b V_b}{n_b z_b} = \frac{P_a \left[V_b + \left(1 - \frac{P_h X_h^w}{P_w}\right) dV_h\right]}{z_a (n_b + \frac{dV_h P_h X_h^m}{M_m})}. \quad (6)$$

In equation (A6), dV_h is the only unknown. By rearranging Equation A6 we obtain

$$dV_h = \frac{(P_a z_b - P_b z_a) n_b V_b}{P_b V_b z_a \frac{P_h X_h^m}{M_m} - P_a n_b z_b (1 - \frac{P_h X_h^w}{P_w})} \quad (7)$$

No heat flow case:

At point c, the gas phase could be described by the gas law as:

$$P_c V_c = n_c z_c R T_c, \qquad (8)$$

where P_c, V_c, n_c, Z_c, and T_c are the pressure, volume of the gas phase, total molar of methane in the gas phase, gas compressibility and temperature at point c, respectively.

P_c can be calculated from the methane hydrate phase boundary

$$P_c = F(T_c, Cl_c), \qquad (9)$$

where F means the methane hydrate phase boundary, and we use the model of Liu and Flemings (2007) to describe it; Cl_c means the system bulk salinity at point c.

V_c can be calculated as

$$V_c = V_b + dV_g = V_b \left(1 - \frac{P_n X_h^w}{P_w}\right) dV_h. \qquad (10)$$

n_c can be calculated as

$$n_c = n_b + dn_g = n_b + \frac{dV_h P_h X_h^m}{M_m}. \qquad (11)$$

z_c is a function of P_c and T_c. One can use a range of models to describe z_c. To be simple, we assume z_c equals z_b in this study. We assume that there is negligible change of the system heat capacity from point b to point c. According to energy conservation, we obtain

$$V_t C (T_b - T_c) = dV_h \rho_h L, \qquad (12)$$

where V_t is the total volume of the system, C is the heat capacity of the system, and L is the latent of hydrate. By rearranging Equation A12, we obtain:

$$T_c = T_b - \frac{dV_h P_h L}{V_t C}. \qquad (13)$$

By substituting Equations 9-11 and 13 into Equation 8, we obtain a nonlinear equation with regards to dV_h,

$$F\left(Tb - \frac{dV_h P_h L}{V_t C}, Cl_c\right) \cdot \left[V_b + \left(1 - \frac{\rho_h X_h^w}{P_w}\right) dV_h\right] = \left[n_b + \frac{dV_h \rho_h X_h^m}{M_m}\right] Z_b R \left[T_b - \frac{dV_h P_h L}{V_t C}\right]. \qquad (14)$$

We can obtain dV_h by solving Equation 14.

3.2.4.2 Core depressurization model

We developed a radial 2D numerical model to predict the behavior of the system during hydrate dissociation in a closed chamber which contains hydrate-bearing core (Figure 3-13). This model is thermodynamic equilibrium-based, which means we neglect any hydrate dissociation kinetics and hydrate dissociation follows the local hydrate phase boundary. We consider the endothermic nature of hydrate dissociation. We assume the temperature at the surface of the chamber is constant and equals the room temperature.

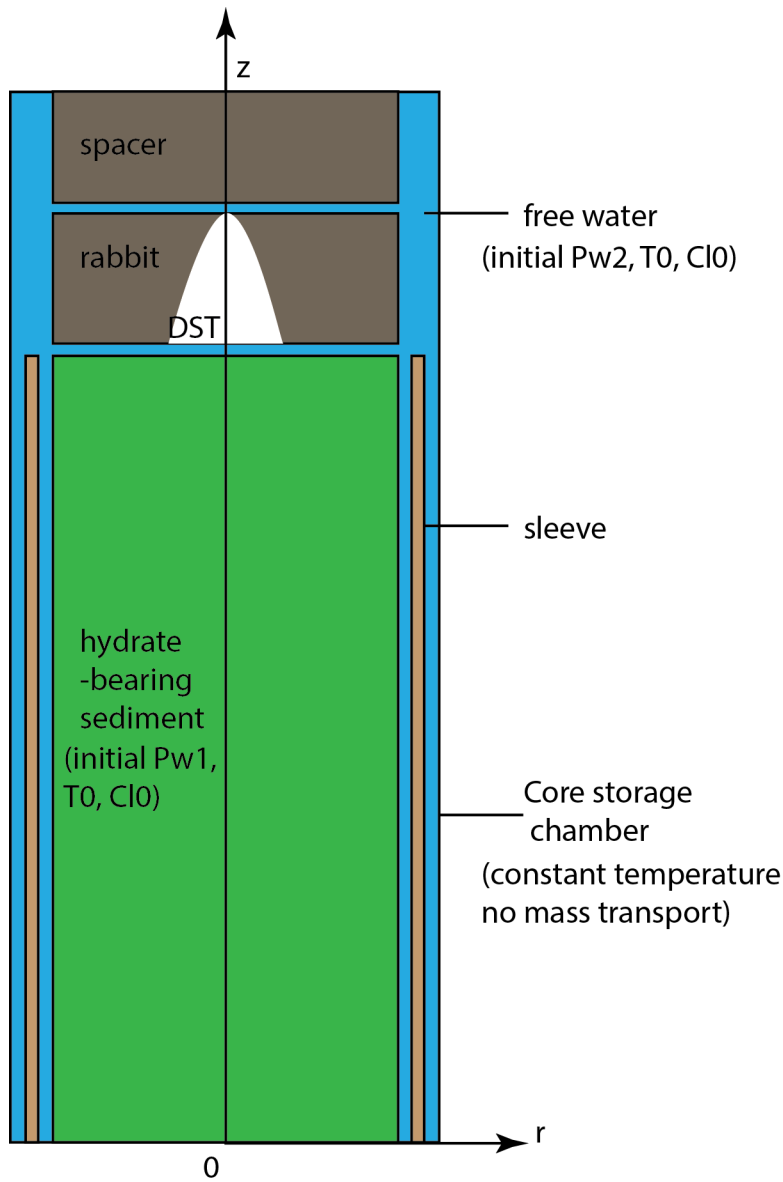

Figure 3-13: Schematic of the 2D radial model for pressure recovery during a shut-in period when a hydrate-bearing core is depressurized. The figure is plotted not to scale. We simulate the space (include spacer, rabbit, DST and free water) above the hydrate-bearing sediment as a homogeneous porous media with a porosity of 0.29 and water saturation of 100%. We simulate the sleeve surrounding the hydrate-bearing sediment as a porous media with a porosity of 0.001 and water saturation of 100%. The intrinsic permeability and effective methane diffusion coefficient of the sleeve is set to be 0.01 and 0.1 of the sediment, respectively. The intrinsic permeability and effective methane diffusion coefficient of the free water surrounding the sediment and the "porous media" above the sediment is set to be 100 times and 10 times of those for the sediment, respectively. The initial condition within the hydrate-bearing core (Pw1, T0, Cl0) is hydrate stable; the initial condition in the free water surrounding the core and the "porous media" above the core is hydrate unstable (Pw2, T0, Cl0), which is used to simulate the condition at the beginning of each shut-in during the depressurization experiment. Pw1 and Pw2 are the water pressure; T0 is the initial temperature; Cl0 is the initial salinity.

Our model include three components (κ), water (w), methane (m) and salt (s), and they can form three phases (β), liquid (l), gas (g) and hydrate (h). The mass conservation equations for water, methane and salt can be described by

$$n\frac{\partial \sum_{\beta=l,g,h} \rho_\beta S_\beta X_\beta^\kappa}{\partial t} - \sum_{\beta=l,g} div\left\{\frac{kk_{r\beta}}{\mu_\beta}\rho_\beta X_\beta^\kappa\left(\nabla P_\beta - \rho_\beta g\right)\right\}$$
$$-div\left\{nS_\beta D_\beta^\kappa \nabla\left(\rho_\beta X_\beta^\kappa\right)\right\} - q^\kappa = 0, \qquad \kappa = w, m, s \qquad (15)$$

where t is time (s); n is porosity (dimensionless); ρ_β and S_β are the density (kg m-3) and saturation (dimensionless) of phase, respectively; X_β^κ is the mass fraction of component in phase (dimensionless); D_l^k is the molecular diffusion coefficients (m^2 s^{-1}) of component κ in the pore water of the sediments, and $D_l^k = n_0 D_{l0}^k$ [Liu and Flemings, 2007]; D_{l0}^k is the molecular diffusion coefficients (m^2 s^{-1}) in free water; q^κ is the source or sink of component κ (kg m^{-3} s^{-1}); μ_β , P_β and $k_{r\beta}$ are the dynamic viscosity (Pa s), pressure (Pa) and relative permeability (dimensionless) of β phase, respectively; g is the acceleration due to gravity (m s-2).

We consider the advective and conductive heat transport, and the latent heat of hydrate formation and dissociation in the free gas flow model. The energy balance equation (superscript e) is described as

$$\frac{\partial\left((1-n)\rho_s C_s T + \sum_{\beta=l,g,h} n\rho_\beta S_\beta u_\beta\right)}{\partial t} - \frac{\partial\left(n\rho_h L_h S_h\right)}{\partial t} + \sum_{\beta=l,g}\nabla\left\{nS_\beta v_\beta \rho_\beta h_\beta\right\} - \nabla\left\{\lambda_{bulk}\nabla T\right\} - q^e = 0 \qquad (16)$$

where the subscript s denotes the solid grain; T is temperature (°C); λ_{bulk} is the bulk thermal conductivity of the porous media (W m^{-1} oC^{-1}), and $\lambda_{bulk} = (1-n)\lambda_R + n\sum_{\beta=l,g,h} S_\beta \lambda_\beta$; λ_β , u_β and h_β are the thermal conductivity (W m^{-1} oC^{-1}), specific internal energy (J kg-1) and specific enthalpy (J kg^{-1}) of phase , respectively; ; q^e is the energy generation rate (J m^{-3} s^{-1}); L_h is the latent heat of hydrate formation and dissociation (J kg^{-1}).

Initially, we set temperature inside the chamber to be homogeneous and equal the room temperature. Salinity inside the chamber to be homogeneous and equals the bulk equilibrium salinity (Figure 3-13). We set the pressure in the hydrate-bearing core to be above the hydrate phase boundary under which condition hydrate is stable (Figure 3-13). We set the pressure in the free water (no sediment) that surrounds the hydrate-bearing core to be below the hydrate phase boundary (Figure 3-13). This will induce hydrate dissociation as the high pressure within the hydrate-bearing sediment dissipates away. As a result, pressure at the top of the chamber (no sediment) gradually increases. As hydrate dissociates, the temperature in the hydrate-bearing sediment decreases. Heat flows into the chamber to further dissociate hydrate and increase the pressure at the top of the chamber.

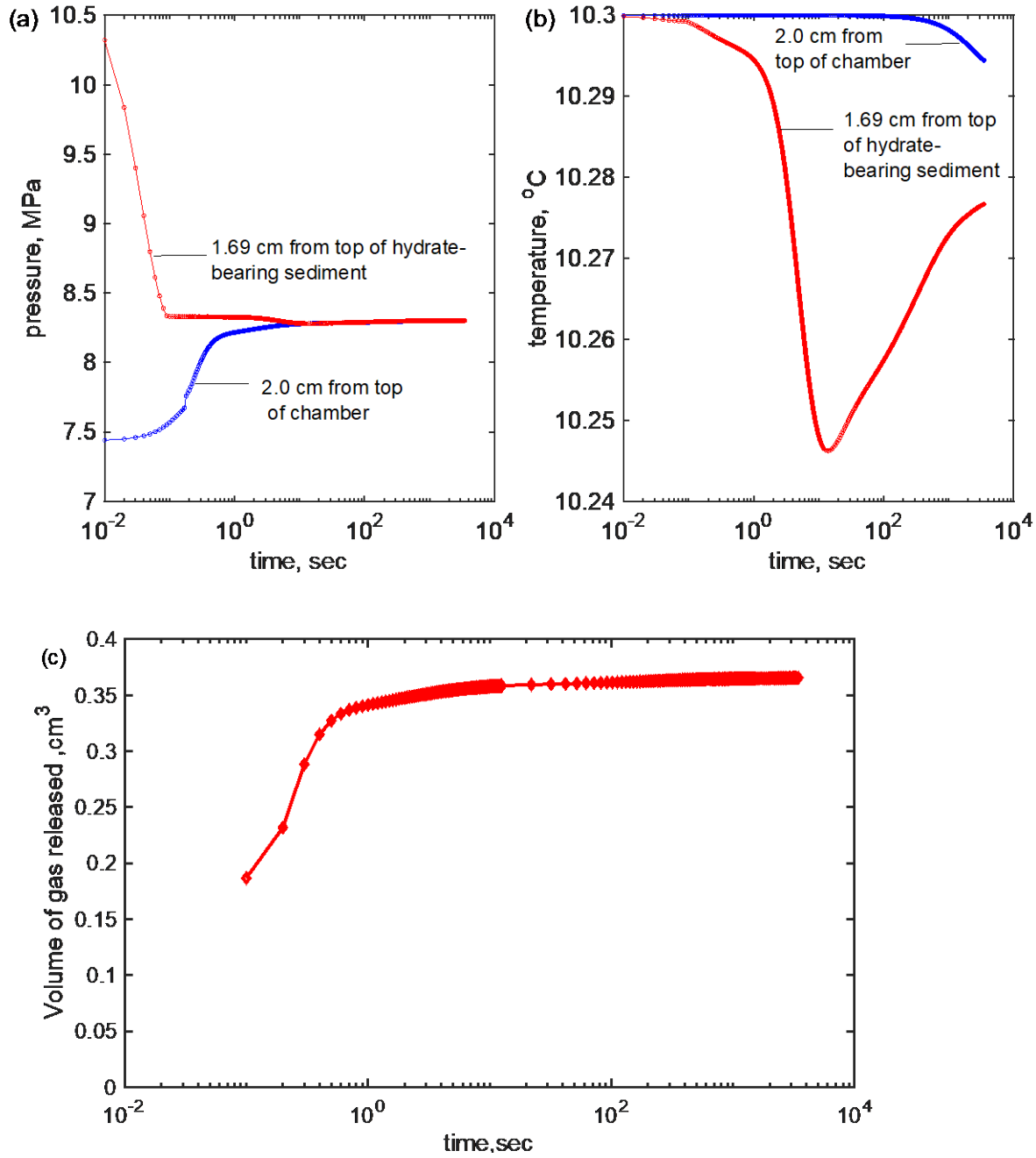

Figure 3-14: Evolution of (a) pressure and (b) temperature at 2.0 cm from the top of the chamber (blue lines) and 1.69 cm from the top of hydrate-bearing sediment (red lines) during a shut-in period. (c) Volume of free gas released in the closed chamber. Hydrate dissociates rapidly at the beginning of shut-in (~0.05 sec to ~ 10 sec) due to pressure dissipation from the hydrate-bearing sediment to the free space; hydrate then dissociates slowly (> ~10 sec) due to heat transfer from outside chamber to the hydrate-bearing sediment. The initial more rapid pressure decreases in the core (a: red line) is the pressure decreasing above the methane hydrate phase boundary (0 to ~0.05 sec). There is no methane hydrate dissociation during this period.

3.2.4.3 Modeling pressure core degradation during storage

We developed a similar 2D radial numerical model as in section 3.2.4.2 to describe the loss of hydrate from hydrate-bearing pressure core during long-term storage. The difference of this model includes: (1) we keep the

temperature within the entire chamber constant and equals room temperature (6 °C); (2) we keep the pressure constant within the entire chamber and equals 24 MPa; (3) the dissolved methane concentration within the hydrate-bearing sediment is in equilibrium with methane hydrate (or equals methane hydrate solubility) and is 0% in all other free space (Figure 3-15 a); (3) the salinity within the hydrate-bearing sediment equals seawater value (3.5 wt.%) and equals 0% in all other free space within the chamber (Figure 3-15 c).

During storage, the diffusion of dissolved methane gradually transports methane from the hydrate-bearing core to the surrounding fresh water within the chamber (Figure 3-15 b). This drives methane hydrate at the top and radial surface of the core to gradually dissolve and hydrate saturation to decrease (Figure 3-15 e, f). At the same time, salt diffuses away from the hydrate-bearing core to the surrounding fresh water (Figure 3-15 d). This decreases the density of the pore water in the core and increases density of the fresh water surrounding the core, which induces density-driven flow of water and accelerates hydrate loss.

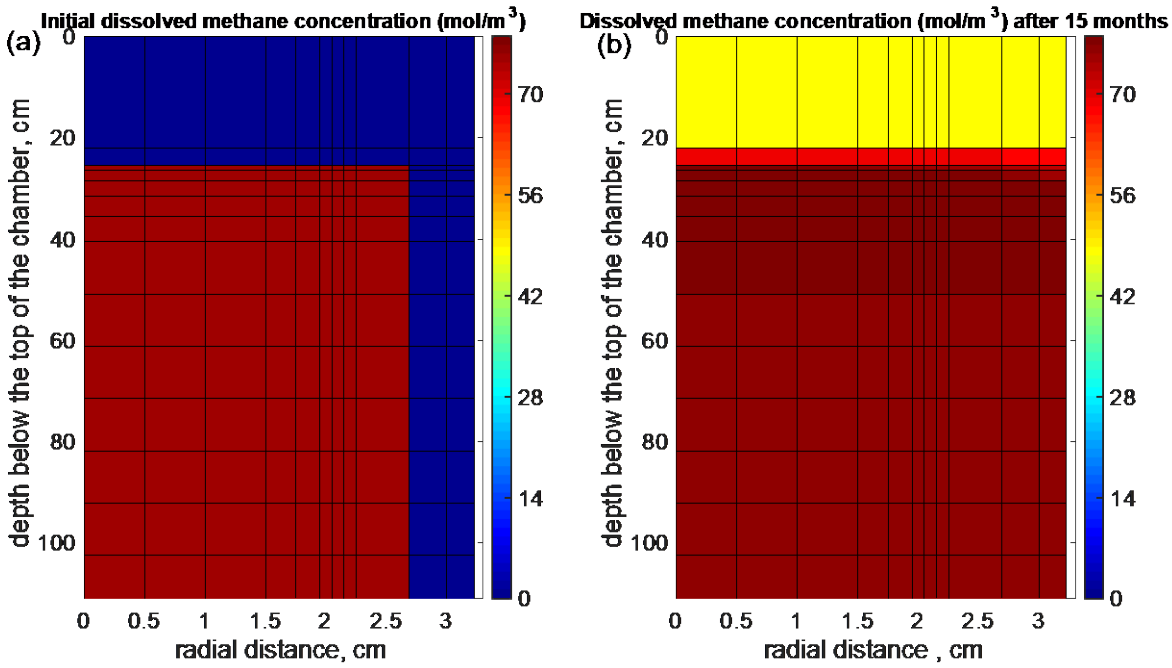

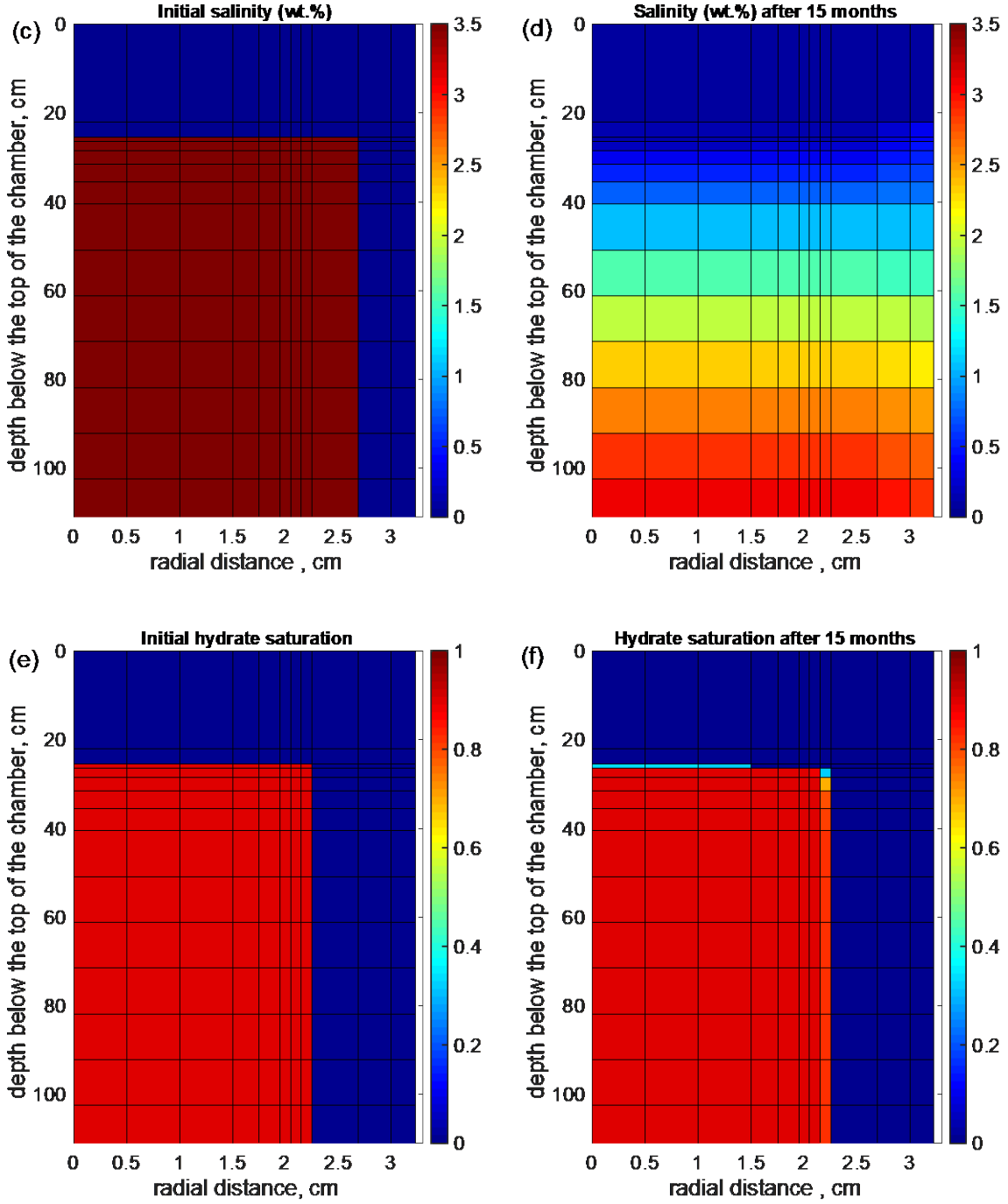

Figure 3-15: Dissolved methane concentration (a, b), salinity (c, d) and hydrate saturation (e, f) at the initial condition and after 15 months of storage at 24 MPa and 6.0 °C.

3.3 Task 11.0: Update Science and Operational Plans for UT-GOM2-2

Objectives

The Recipient will continue to develop, in consultation with the project Advisory Team, the pre-expedition drilling / logging / coring / sampling Operation Plan for the UT-GOM2-2 Scientific Drilling Program. The Recipient will document the developed Operational Plan as a dedicated Operational Plan report.

Additionally, the Recipient will continue to conduct science and sample distribution planning for the UT-GOM2-2 Scientific Drilling Program. A Science and Sample Distribution Plan will be developed that defines the UT-GOM2-2 Scientific Drilling Program science objectives; details sample acquisition, processing, preservation and distribution plans; clarifies container movement and activity; provides detailed equipment and inventory lists, and documents science party requirements.

Accomplishments

3.3.1 UT-GOM2-2 Operations Plan

The UT-GOM2-2 Operations Plan was updated throughout BP4 to reflect changes made to the BOEM Exploration Plan, Science and Sample Distribution Plan, and final schedule and resource estimates.

UT and Ohio State developed an Addendum to the UT-GOM2-2 Operations Plan to include two up-dip locations, WR313 F001 and WR313 F002. With current funding, UT-GOM2-2 will core two wells at two locations in the Gulf of Mexico. It was mutually determined by UT and DOE that two additional wells would be permitted: a logging-while-drilling (LWD) well, and a cored well, at an up-dip location. This will allow for the opportunity to drill additional wells and completed more of the original science objectives, should additional funding become available prior to UT-GOM2-2 execution.

3.3.1.1 Drilling Fluid Planning

A proposal for the use of salt-saturated, water-based drilling mud was submitted to UT as a consideration for UT-GOM2-1. The additional salt moves the hydrate stability boundary to close to our estimated coring conditions and does not give us enough room to operate. Figure 3-16 plots the in situ and expected borehole temperatures for WR313 (UT-GOM2-2) and GC955 (UT-GOM2-1) against the hydrate stability boundary for different salinities (dashed lines). The distance between the estimated borehole temperature and the hydrate stability boundary for the salinity proposed (Figure 3-16, large light blue arrows) indicate how large of a temperature increase that can be tolerated before the pressure core might be compromised (degraded). The window for WR313 is smaller than the expected temperature rise as estimated from temperature swings measured at GC 955. More details can be found in *DE-FE0023919 Quarterly Research Performance Progress Report (Period Ending 09/31/20), Attachment A: Technical Note - UT-GOM2-2 Drilling Fluid.*

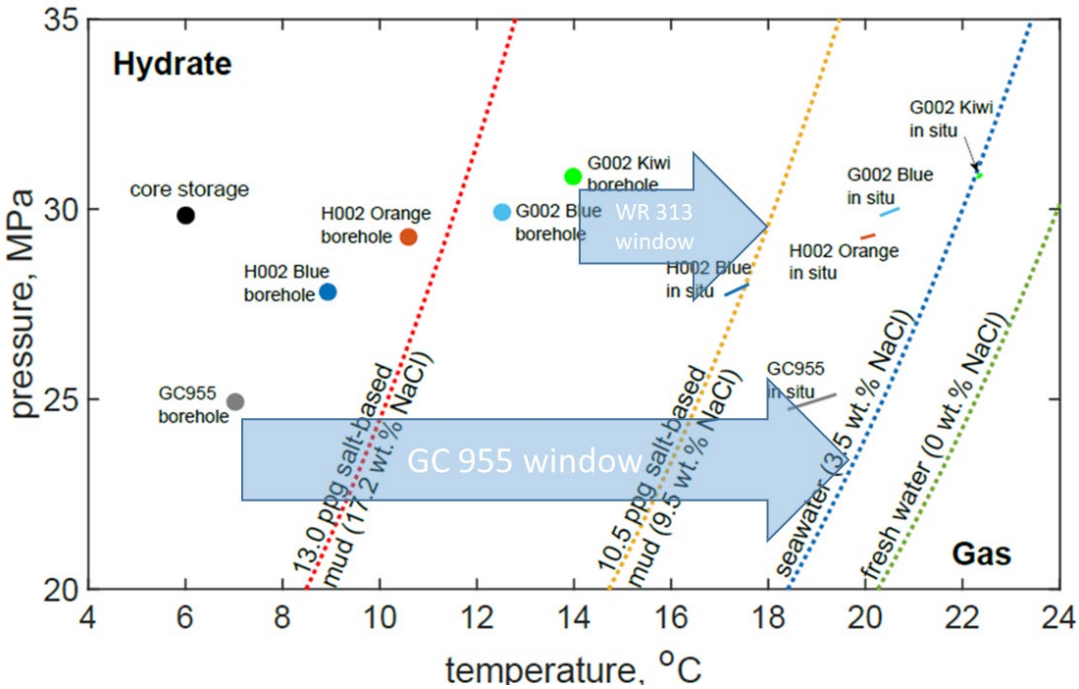

Figure 3-16: Methane hydrate phase diagram for different salinities. The dotted green, blue, orange and red lines are the methane hydrate phase boundaries for fresh water (0 wt.% NaCl), seawater (3.5 wt.% NaCl, the assumed in-situ salinity), 10.5 ppg salt-based mud (9.5 wt.% NaCl) and 13.0 ppg salt-based mud (17.2 wt.% NaCl), respectively. Methane hydrate is stable to the left of the phase boundary and unstable to the right. The solid light blue and orange lines are the in situ conditions for the H002 Blue and Orange sands, respectively. We used the temperature LWD borehole temperature to estimate the coring borehole temperature. The pressure gradient is 0.465 psi/ft. The solid dots are the estimated borehole temperatures and pressures while coring for each sand. The large blue arrows highlight the amount of temperature increase that can be tolerated as the core is brought from the bottom of the hole to the rig floor. The hydrate phase boundaries are calculated by the models presented in Liu and Flemings (2007). The black dot shows the expected pressure and temperature conditions for off-shore core storage of 6 oC (42.8 F) and 30 MPa (4351 psi).

3.3.2 UT-GOM2-2 Science and Sample Distribution Plan

Version 1 of the UT-GOM2-1 Science and Sample Distribution plan was released and reviewed by the GOM2 Technical Advisory Group (TAG, members Ray Boswell, Tim Collett, Steve Phillips, Bill Waite, Yongkoo Seol, Sheng Dai, Peter Flemings, Carla Thomas). An updated plan (Version 2) was started based on feedback from the TAG and others. The plan contains: a review of the science objectives with rationale and the specific plan to meet each objective (~15 pages), the detailed Coring Plan including core points with LWD logs from JIP II, on-board and Dockside Pressure and Conventional Core analyses and sample allocation/movement, required equipment and personnel, a rough Appendix for Detailed methods and analytical descriptions, an appendix describing modification to the plan should additional holes be budgeted and approved by the DOE, and an appendix describing modification to the plan to compensate for the possible Cook APL.

The following specific recommendations from the TAG were captured:

- Prioritize the allowance PC pair above the Blue sand (Blue sand seal) in H002. Great opportunity here for many aspects of the program.
- Check in with Geotek on best shallow pressure coring technique – maybe operate PCTB like a push corer: low rotation, low flow rates

- Make sure there is a component contrasting conventional vs pressure cores for microbiological research – opportunity to study the effect of pressure on microbiology
- Check with Rick Colwell and others on the opportunity to collect samples from pressure cores using Geotek's LN2 apparatus at the dock
- All XRD samples should go to the same lab; include detailed clay analysis of all major units (in triplicate)- James Hutton Institute
- All post-expedition laser particle size grain size measurements should be done at the same lab - UNH, settling method grain size measurements need to be done at UT
- Make sure we have supplies and protocols in place for collecting gas hydrate samples from conventional core
- Take vane shear measurements on the ends of cores on-board and at the dock

3.4 Task 12.0: UT-GOM2-2 Scientific Drilling Program Vessel Access

Objectives

If the CPP is not forwarded to the JRFB (or in parallel with the CPP process if deemed to be needed by mutual agreement of Recipient and DOE), the Recipient, in coordination with the project Advisory Team, will investigate alternate potential means of gaining access to a mutually acceptable vessel suitable for conducting the planned UT-GOM2-2 Scientific Drilling Program. This may include, but is not limited to, the Recipient contracting a vessel independently, investigating plausibility of accomplishing drilling program with 'vessels of opportunity' as directed by DOE.

Accomplishments

UT will independently contract a fit-for-purpose deepwater drilling or intervention vessel for UT-GOM2-2. In BP4, UT initiated weekly Vessel Procurement team meetings, to determine vessel requirements, develop and integrate information required for solicitation, and to determine the vessel procurement strategy.

UT conducted extensive analysis of drilling/coring/operations time and resources, and developed a refined offshore operations schedule based on updated information from the project teams responsible for the UT-GOM2-2 Science and Sample Distribution Plan, UT-GOM2-2 Operations Plan, and UT-GOM2-2 BOEM Exploration Plan. Time and resource estimates were developed for the base plan, as well as for alternative scenarios including those allowing time for allowance cores, contingency scenarios, and for cases in which the 4-well UT-GOM2-2 program is executed.

UT requested and received draft mud volume estimates and quotes from MI SWACO based on the drilling programs, and refined the estimates based on our institutional knowledge of coring in the GOM (e.g. JIP, GC-955)

UT developed two documents for prospective vessel contractors, based on the most recent operations and science plan requirements, and with input from DOE, USGS, BOEM, and Geotek:

1. Vessel Specification

    a. Details technical specifications required for a vessel to meet the UT-GOM2-2 objectives
2. Well Design
    a. Provides a high level overview of the project with emphasis on information useful for potential vessel contractors. This document draws largely from the UT-GOM2-2 Operations Plan and time estimates for WR313-H002, WR313-G002, WR313-F001 and WR313-F002.

The documents were finalized and provided to prospective vessel contractors. The purpose of the specifications is to stimulate technical discussions around fit-for-purpose concerns. The intended targets of the updated specifications were contractors of smaller vessels (intervention / geotechnical vessels).Larger drilling rigs will easily meet the technical specifications of our project. It was not seen as necessary to send updated specifications for the purpose of determining fit-for-purpose suitability to contractors of the big drilling vessels. Requests for quote will be sent out after fit-for-purpose concerns have been evaluated and the list of potential contractors is determined.

3.5 Task 13.0: Maintenance and Refinement of Pressure Core Transport, Storage, and Manipulation Capability

3.5.1 Subtask 13.1: Hydrate Core Manipulator and Cutter Tool

Objectives

The Recipient will maintain the ability to use the Manipulation and Cutting Tool (developed under Phase 2, Subtask 9.5) and implement appropriate design modifications to improve the capability of the tool as determined to be necessary by mutual agreement of the Recipient and DOE.

Accomplishments

UT maintained active utilization of the Mini-PCATS and associated equipment to advance the laboratory-based experiments and pressurized core sample distribution:

- **Period ending December 31, 2019:**
  - Two cores were scanned and subsampled with the aid of the new CT scanner system:
    - Core H005-7FB-3: Two K_0 samples
    - Core H002-4CS-2: One Degas sample
  - AIST Storage Chambers:
    - Two storage chambers were held at pressure
    - Two chambers with samples were picked up by Geotek and placed into the Overpack Reefer Unit for shipment to Japan on December 20, 2019
- **Period ending March 31, 2020:**
  - One core was scanned and subsampled with the aid of the new CT scanner system:
    - Core H005-7FB-3: Two K_0 samples
    - Core H005-7FB-3: Natural Hydrate Raman Spectroscopy Chamber sample
      - On March 12, 2020, the first micro-Raman scanning was conducted on a WR313 methane hydrate sample. Raman spectra was obtained.
    - Core H005-7FB-3: Degas sample
- **Period ending June 30, 2020:**
  - One core was scanned and subsampled with the aid of the new CT scanner system:
    - Core H005-7FB-3: One K_0 sample, two degas samples (one bulk gas, one rapid)
- **Period ending September 30, 2020:**
  - One core was scanned and subsampled with the aid of the new CT scanner system:
    - Core H005-2FB-2: One K_0 sample

UT conducted regular system maintenance and teardowns of the Mini-PCATS cutter, rotation, and viewing units after sample cutting. The system was cleaned and cutter blades replaced after each sampling. UT also conducted bi-annual teardowns of the Power Balance Drive for preventative maintenance.

All teardowns have the following steps:

- Removal of sediment from sample cutting
- Removal and mitigation of corrosion
- Complete replacement of all bearings, seals, and O-rings

- Lubrication of necessary bearings and components

3.5.2 Subtask 13.2: Hydrate Core Effective Stress Chamber

Objectives

The Recipient will maintain the ability to use the Effective Stress Chamber (developed under Phase 2, Subtask 9.6) and implement appropriate design modifications to improve the capability of the tool as determined to be necessary by mutual agreement of the Recipient and DOE.

Accomplishments

UT maintained active utilization of the hydrate core effective stress chamber and associated components to advance laboratory-based experiments:

- **Period ending December 31, 2019:**
  - Two pressure core samples underwent K_0 testing:
    - H005-7FB-3-1
    - H005-7FB-3-2
- **Period ending March 31, 2020:**
  - Two pressure core samples underwent K_0 testing:
    - H005-7FB-3-3
    - H005-7FB-3-4
- **Period ending June 30, 2020:**
  - One pressure core sample underwent K_0 testing:
    - H005-7FB-3-5 – Viton sleeve failed to seal, sample tested using new Geotek procedures. Sample was degassed in K_0.
- **Period ending September 30, 2020:**
  - One pressure core sample continues to undergo long-term K_0 testing:
    - H005-2FB-2 – Sample subjected to permeability testing with the presence of hydrate. The hydrate was then dissolved out of the sample while maintaining an axial load and radial effective stress. The sample will next undergo permeability testing without the presence of hydrate.
  - System underwent cleaning between tests. All seals were replaced.

UT conducted regular system maintenance of the hydrate core effective stress chamber and related components. The hydrate core effective stress chamber and actuator motor were disassembled, cleaned of all debris, replaced seals and O-rings, and reassembled as needed. Test sections were cleaned and reset as needed.

In March, 2020, UT identified several operational deficiencies in the K_0, including scratches on sealing surfaces, bottom cap seal failures, increased motor torque, and reduced axial loading capability. UT held technical conference with Geotek on these issues. Geotek provided a series of procedures intended to remedy these issues.

From April through June, 2020, UT conducted three dummy sample tests using new procedures suggested by Geotek. The new procedures resulted in achieving better alignment of components during sample extrusion, enabled successful bottom cap sealing in clean environments (no sediment), and axial loading via hydraulic pressure (up to 9-10 MPa). This has reduced motor torque, eased extrusion, and appears to have eliminated scratching on sealing surfaces. However, during axial loading via the bottom cap/hydraulic pressure combination, it was discovered that the K_0 load cell had reached the maximum of its measurement range.

After testing the updated K_0 testing procedures on three dummy sample tests, the procedures were applied to pressure cores:

- H005-7FB-3-5: The sample was extruded with low motor torque. However, we were unable to seal the sample sleeve and the bottom cap. The failure to seal the bottom cap prevented axial loading of the sample via hydraulic pressure behind the bottom cap. In addition, the bottom cap was fitted with plastic X-ring seals instead of O-ring seals. After the 7FB-3-5 K_0 test was conducted, the X-ring seals were found to have significant distortion. This follows with the observed sealing failure of the bottom cap.
- H005-2FB-2: Scratching and high torque values were not exhibited. However, UT was unable to achieve sealing of the K_0 bottom cap and achieve hydraulic axial loading.
- H005-2FB-2-1: The sample was extruded with low motor torque. We were able to seal the sample sleeve but unable to seal the bottom cap. The failure to seal the bottom cap prevented axial loading of the sample via hydraulic pressure behind the bottom cap. The bottom cap was fitted with standard O-ring seals. The test is still ongoing.

Testing and evaluation is ongoing to identify the proper type of seals and procedures necessary to allow sealing of the bottom cap in a pressure core environment. Once bottom cap sealing has been achieved, axial loading of a pressure core sample will be tested using hydraulic pressure.

3.5.3 Subtask 13.3: Hydrate Core Depressurization Chamber

Objectives

The Recipient will maintain the ability to use the Depressurization Chamber (developed under Phase 2, Subtask 9.7) and implement appropriate design modifications to improve the capability of the tool as determined to be necessary by mutual agreement of the Recipient and DOE.

Accomplishments

UT continued to utilize and refine their capability to use the hydrate core depressurization chamber:

- **Period ending December 31, 2019:**
  - H002-4CS-2 – Degassed
- **Period ending March 31, 2020:**
  - H005-7FB-3-6 was prepared for degassing
- **Period ending June 30, 2020:**
  - H005-7FB-3-6 – Degassed

- H005-7FB-3-7 – Underwent slow, bulk gas sample degassing
- H005-7FB-3-8 – Final remnant of 7FB-3 prepared for rapid degassing

- **Period ending September 30, 2020:**
  - H005-7FB-3-8 – Final remnant of 7FB-3, underwent rapid degassing
  - The system was used to quantify dissolved and dissociated methane hydrate from H005-2FB-2.

3.5.4 Subtask 13.4: Develop Hydrate Core Transport Capability for UT-GOM2-2

Objectives

The Recipient will continue to refine, maintain and /or develop the ability to transport pressure cores, as determined to be necessary through mutual determination of the Recipient and DOE, for the core to be acquired in Phase 5 (Task 16) of the project.

Accomplishments

UT continued to assess current capabilities and requirements for transporting pressure cores that will be acquired in during UT-GOM2-2 based on the revised UT-GOM2-2 Science Plan and Operations Plan.

3.5.5 Subtask 13.5: Expansion of Pressure Core Storage Capability for UT-GOM2-2

Objectives

The Recipient will develop capacity to store pressure cores resultant from the Research Expedition in Phase 4 (Task 16) of the project. The Recipient will identify a specific technology for storing pressure core at research institutions in the United States. The Recipient will either build or lease the capability to store a minimum of 36 meters of pressure cores.

Accomplishments

UT continued to assess current capabilities and requirements for storing pressure cores that will be acquired in during UT-GOM2-2 based on the revised UT-GOM2-2 Science Plan and Operations Plan.

- A new core chamber orientation has been designed to accommodate UT-GOM2-2 cores, that requires manufacturing of new chamber supports. UT has obtained and is reviewing quotes.
- Expansion of the pressure maintenance system is required to increase storage capability sufficient to receive UT-GOM2-2 cores. UT has obtained and is reviewing quotes for additional pressure lines.
- Expansion of pressure safety venting system will also be required to increase storage capability. UT has obtained and is reviewing quotes for additional venting lines.

3.5.6 Subtask 13.6: Continued Storage of Hydrate Cores from UT-GOM2-1 Marine Field Test

Objectives

The Recipient will continue to store (under hydrate stable conditions) pressure core acquired from UT-GOM2-1 Marine Field Test in Phase 2 (Task 8).

Accomplishments

UT continued to store, stabilize, and perform tests on pressure core acquired from the UT-GOM2-1 Marine Field Test (May-June 2017).

- UT performed weekly pressure checks on pressure chambers.
- UT completed drawings to redesign the pressure chamber storage bases to increase capacity.
- UT completed a preliminary budgetary analysis to expand the pressure, maintenance, and relief system (PMRS) to accommodate the increased capacity described above.

Core storage expansion in the PCC is anticipated to accommodate any remaining pressure cores acquired from UT-GOM2-1 once additional cores are collected during UT-GOM2-2 and transferred to the PCC.

3.5.7 Subtask 13.7: X-ray Computed Tomography

Objectives

The Recipient will maintain the ability to use the X-Ray CT developed in Phase 3, Subtask 9.8 and implement appropriate design modifications to improve the capability of the tool as determined to be necessary, by mutual agreement of the Recipient and DOE.

Accomplishments

The X-Ray CT continues to operate as designed. UT continued to perform preventative maintenance and cleaning of the X-Ray CT system on Mini-PCATS. The system was cleaned of sediment, seals were replaced, and imaging system calibrated. The system undergoes a yearly radiation survey to ensure lead cabinet is remaining sealed when X-rays are being discharged during CT scanning.

3.5.8 Subtask 13.8: Pre-consolidation System

Objectives

The Recipient will maintain the ability to use the Pre-Consolidation System developed in Phase 3, Subtask 9.9 and implement appropriate design modifications to improve the capability of the tool as determined to be necessary by mutual agreement of the Recipient and DOE.

Accomplishments

UT conducted standard maintenance of the system including cleaning and flushing of the system. During routine inspection, one of the Pre-Consolidation System hydraulic accumulators developed a leak at the gas charging port. This prevents charging the accumulator with nitrogen to allow for hydraulic pressurization and sample storage. It was discovered that the gas port had damaged O-rings and a stuck spring. New O-ring seals are being sourced, and replacement parts have been quoted and ordered from Geotek.

3.6 Task 14.0: Performance Assessment, Modifications, and Testing of PCTB

3.6.1 Subtask 14.2: PCTB Modifications/Upgrades

Objectives

The Recipient will recommend modifications and/or upgrades of pressure coring and core analysis tools to assure the readiness of the system for use in the UT-GOM2-2 Scientific Drilling Program during Phase 5, Task 16, based on the outcomes of the PCTB Lab Test (Subtask 14.1) and in coordination with DOE and the Project Advisory Team. The recommended modifications will be implemented based on the outcomes of the laboratory-based testing and by mutual agreement of the Recipient, DOE and the Project Advisory Team.

Accomplishments

In January, 2020 Geotek completed upgrading the upper section of the PCTB to address issues of late sealing and unrealized pressure boost experience during UT-GOM2-1. UT Austin, with consultation from DOE and the PCTB Development Team, approved six modifications to the PCTB Mk. 3, based on the results and analysis of the of PCTB bench tests performed by Geotek in April-May, 2019. Geotek completed upgrading all PCTB Mk. 4 tool sets to PCTB Mk. 4 specifications in January, 2020. The following modifications were made:

1. Single-Trigger Mechanism
    a. A single-trigger mechanism replaced the original complex vent port mechanism which relied on an O-ring face seal to complete the autoclave upper sealing mechanism. The original vent port closing actuation timing was controlled by a spring and was very close to that of firing the boost which led to potential loss of the boost pressure. The single trigger mechanism makes it impossible for the boost to fire prior to closing the vent port while eliminating the O-ring face seal and spring.
2. Low Friction Coatings
    a. All sliding parts and the latch mechanism now have a low friction coating applied to them, to reduce the wireline overpull required to release the PCTB latch from the bottom hole assembly (BHA).
3. IT Plug Mandrel Shear Pin
    a. With the introduction of the single trigger mechanism the IT plug mandrel locking dogs were replaced by a shear rod. The shear rod shear force must be high enough to ensure the autoclave upper seals are properly engaged while low enough to allow the over travel spring to function without prematurely unlatching the PCTB from the BHA.
4. Flow Diverter Seals
    a. Introduction of the single trigger mechanism required the flow diverter to be modified. Part of the diverter modification included replacing the original lip seals with point seals in an effort to increase reliability of the diverter.
5. Regulator Sub
    a. The regulator sub was modified so seal cannot cause hydraulic lock.
6. Pressure Section Increase

a. The pressure section length was increased by 24 inches, more than doubling its volume. The increased volume will ensure adequate high pressure gas is available to activate the autoclave boost in high hydrostatic pressure environments.

3.6.2 Subtask 14.1: PCTB Lab Test

Objectives

The Recipient will perform laboratory-based testing of the PCTB to discover the range of conditions in which pressure retention is inconsistent, duplicate and analyze difficult unlatching scenarios, analyze performance of the inner tube plug, and analyze performance of inner and outer latch systems to obtain a high degree of confidence in overall PCTB operation. Testing will include, but is not limited to, a Pressure Function Testing (PFT) and Pressure Actuation Testing (PAT). Computational Fluid Dynamics modeling will also be conducted to simulate tool response under field conditions. As a result of tool performance during this testing, the Recipient will recommend modifications and/or upgrades of the PCTB to be conducted in Task 14.2.

Accomplishments

Bench tests of the PCTB Mk. 4 were performed at the Geotek high-pressure testing facility in Salt Lake City, Utah, from January 27-31, 2020 (PCTB Bench Test II). The purpose of the PCTB Bench Test II was to confirm that the upgraded PCTB Mk 4. (Subtask 14.2: PCTB Modifications/Upgrades) performed as intended in a controlled environment prior to land testing at Schlumberger CTTF (Subtask 14.3: PCTB Land Test II).

PCTB Bench Test II Pressure actuation tests (PAT) of the PCTB were conducted in which the PCTB was actuated at field-like pressures in Geotek's pressurized test chamber. Fresh water and drilling mud were used in the pressure actuation tests. Twelve PATs were performed. In 10 out of 12 tests, a pressure boost was recorded and pressure was maintained until tool recovery. In the 2 failed tests, operator error caused the PCTB to be assembled incorrectly resulting in failure to seal. The operator errors were identified, documented, and the procedures were corrected.

The Probe Deployment Tool (PDT) and Temperature Pressure Probe (T2P) were also tested. The PDT had not yet been tested in a borehole setting and the T2P's logging electronics have been overhauled since its last field deployment.

Two PDT deployment tests were performed with the T2P attached. The first test was successful. In the second test, the PDT/T2P assembly hung up when it was being pulled out. Hammering and raising/lowering the tool several times freed the tool. Visual inspection of the PDT revealed that all three of the locking dogs were bent and one of the upper latch dogs was missing. It was theorized that the missing latch dog prevented the tool from being pulled out of the test chamber. The latch dogs were refabricated from stronger material for the PCTB Land Test II at CTTF (Subtask 14.3: PCTB Land Test II).

The PCTB Bench Test II report can be found in *DE-FE0023919 Quarterly Research Performance Progress Report (Period Ending 03/31/20), Appendix A: PCTB Bench Test II Report.*

3.6.3 Subtask 14.3: PCTB Land Test II

Objectives

The Recipient will perform a land-based test of the DOE PCTB similar to that conducted previously in Phase 2, Subtask 7.2. This test will be conducted on land at a test facility borehole that is mutually acceptable to DOE and the Recipient. The coring interval will be chosen to be within an interval of the borehole determined to suitably reflect conditions similar to reservoir sands that are saturated with hydrate.

The Recipient will complete all necessary NEPA documentation for the specific site / location to be included as part of the land test of the PCTB pressure coring system and / or any other necessary project tools. Land test activities shall not be conducted until an appropriate final NEPA determination is issued by the DOE / NETL NEPA compliance office.

The Recipient will document the process and results of the PCTB Land Test and report that information to DOE via a dedicated Land-Based Pressure Coring Field Test Report.

Accomplishments

Full-function field tests of the PCTB Mk. 4, the Probe Deployment Tool (PDT), and the Temperature-2-Pressure (T2P) probe were performed at the Schlumberger Cameron Test and Training Facility (CTTF) from March 9-20, 2020 (PCTB Land Test II). Representatives from UT Austin, Geotek Coring Inc., and Pettigrew Engineering participated in the testing.

The primary objectives of the PCTB Land Test II were to determine if the PCTB Mk. 4 functioned as designed in a field environment, and to assess if the Mk. 4 upgrades improved tool performance. Prior to the PCTB Land Test II, the PCTB had been upgraded to Mk. 4 specifications (Subtask 14.2: PCTB Modifications/Upgrades). The PCTB Mk. 4 was then successfully bench tested in a controlled environment at the Geotek high-pressure testing facility (Subtask 14.1: PCTB Lab Test). However, the PCTB Mk 4. had not yet been tested in field conditions.

A secondary objective was to test the Probe Deployment Tool (PDT), to determine if it would function as intended in a field environment. The PDT had not yet been tested in a borehole setting and the T2P's logging electronics have been overhauled since its last deployment.

The PCTB Land Test II report can be found in *DE-FE0023919 Quarterly Research Performance Progress Report (Period Ending 06/30/20), Appendix A: PCTB Land Test II Report.*

PCTB Land Test II: PCTB Full Function Tests

Seven full function tests of the PCTB were performed. Two coring tests were performed with the face bit version (PCTB-FB): CTTF-01FB, CTTF-02FB. This was followed by four coring tests with the cutting shoe version (PCTB-CS): CTTF-03CS, CTTF-04CS, CTTF-05CS, CTTF-06CS. One 'water core' of the PCTB-CS was performed wherein the PCTB was deployed within the casing without coring (CTTF-07CS). After PCTB testing was complete, the PDT with the T2P attached was deployed to assess performance in field conditions.

Core recovery and core quality were high with both configurations of the PCTB (Figure 3-17). Core recovery was generally 80% or higher. In the two runs of the PCTB-FB, the recovery was 83 and 91%, respectively, for core

throws of 6.6 and 9.8 ft. In two long core throws of the PCTB-CS (9.5 and 3.5 ft) the recovery was 79 and 80%. For two short core throws of the PCTB-CS the recovery was more variable (0-197%). There appears to be little difference in recovery between configurations of the PCTB. Core quality was high in both PCTB configurations (Figure 3-17). The diameter of the core was consistent in all cores of both configurations, even across transitions between limestone and shale. Grooves on the exterior of the core were minimal. Core 'biscuiting' was common with core biscuits ranging from cm to tens of cm in length.

We interpret that the addition of the diverter system, which allowed for higher pump rates, resulted in increased penetration rate, increased core recovery, and improved core quality with both the CS and FB PCTB systems.

Figure 3-17: Core CTTF-02FB contained 8.9 ft of limestone and shale after recovery (91% recovery).

The first full function PCTB coring test with the PCTB-FB version (CTTF-01FB) was successful. In this test, a clear pressure increase was recorded when the tool sealed (Figure 3-18).

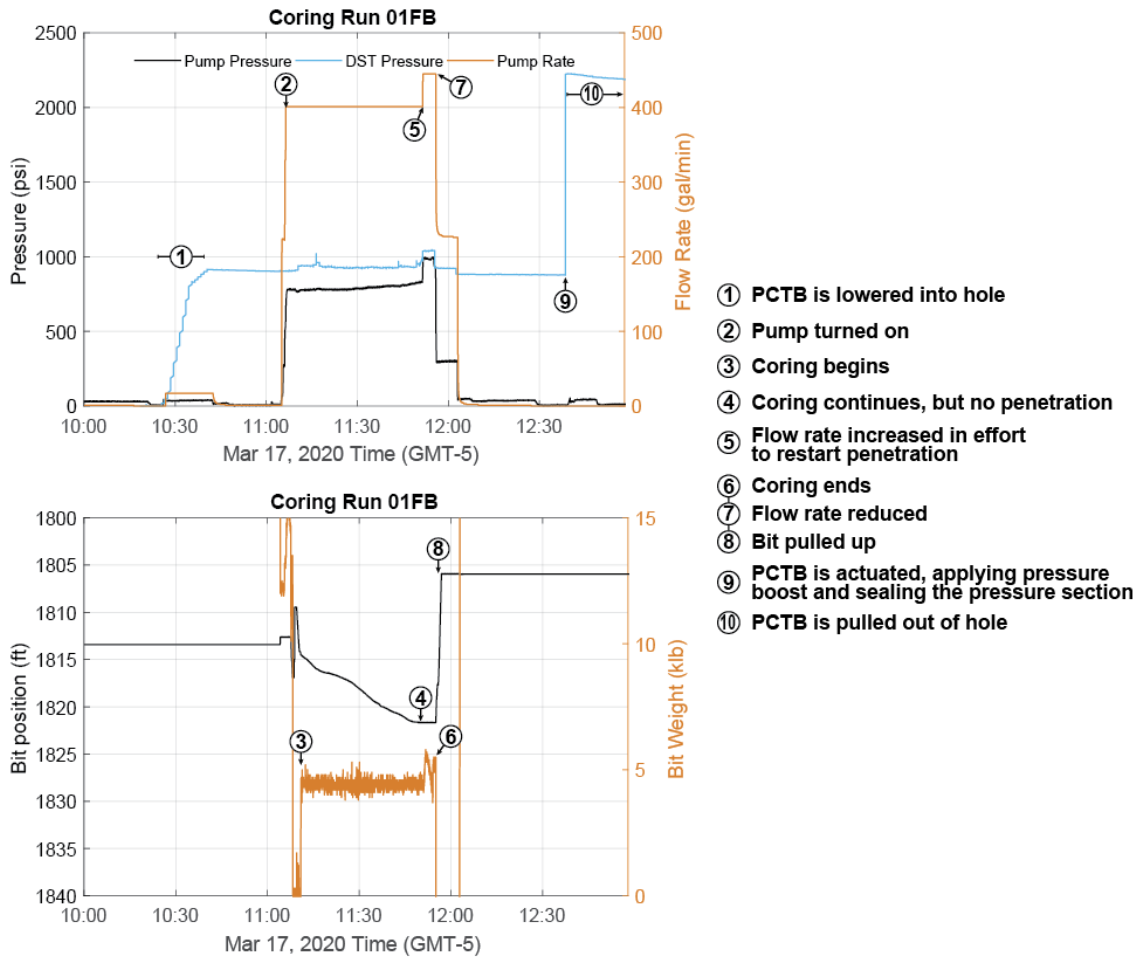

Figure 3-18: DST and rig instrumentation plots for core CTTF-01FB. The PCTB tool boosted and sealed correctly, and pressurized core was recovered.

The PCTB failed to properly seal in each the six subsequent PCTB coring tests, with both the CS and FB versions: CTTF-02FB, CTTF-03CS, CTTF-04CS, CTTF-05CS, and CTTF-06CS. In some cases, the ball valve was observably partially open when the tool was recovered to the surface (Figure 3-19). In other cases, the ball valve appeared closed at the surface (Figure 3-20), however the autoclave did not seal and no boost pressure was recorded. We interpret that in cases where the ball valve appeared sealed at the surface, the ball sealed only after the boost was fired, while being recovered.

Figure 3-19: Partially closed ball valve after recovery from the hole. The red object is the seal carrier. The object opposite the seal carrier, to the right of the ball valve, is the ball follower. When the PCTB is actuated, a spring to the left of the seal carrier drives the ball downward (to the right). When the ball is forced downwards, it rotates around a pin into the closed orientation, sealing the autoclave.

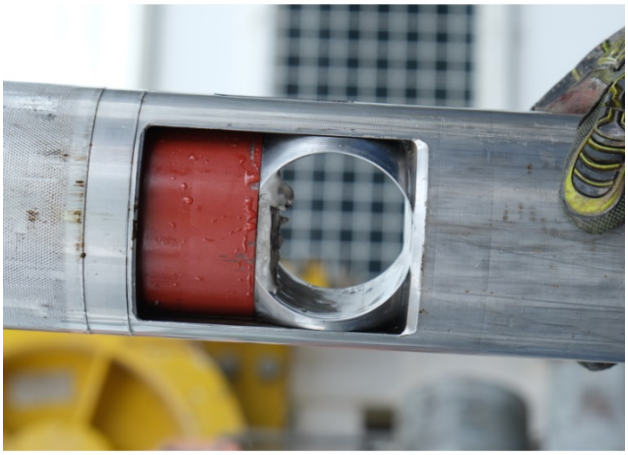

Figure 3-20: Apparently closed ball valve upon recovery from the hole. Although it is apparently sealed, no pressure was held. It is interpreted that either it was a leaky seal or that the ball valve closed after the pressure was boosted. Note the mud and silt between the ball and the seal carrier (red).

We interpreted that the primary failure mode encountered during the PCTB Land Test II was grit from drilling fluid and entrained cuttings becoming wedged between the outer housing and the seal carrier, and/or the outer housing and the ball follower. The PCTB-CS and PCTB-FB sealed consistently during downhole testing in Salt Lake City (Subtask 14.1: PCTB Lab Test). However, this mud did not have detritus or grit within it. The only change in the ball closure mechanism between the Salt Lake City Bench test and the Cameron test was that was to put a low friction coating on it. This was fully vetted in the Bench Test II in Salt Lake City, Utah with no issues.

The PCTB Land Test II provided additional operational experience with the PCTB tools in a wellbore environment. Incremental improvements to the PCTB have improved the reliability of the upper pressure seal. We interpret that the addition of the diverter system to the PCTB Mk 4., which allowed for higher pump rates,

resulted in increased penetration rate, increased core recovery, and improved core quality with both the PCTB-CS and PCTB-FB systems. We also interpret that the implementation of a single trigger mechanism has made the upper seal more reliable.

The PCTB Land Test II clearly delineated that there continues to be a problem with sealing of the ball valve itself, and that this was likely the cause of the late seals or failures to seal in the 2017 UT-GOM2-1 Marine Field Test (Thomas et al., 2020). Grit had been observed in the ball valve assembly failed before, but it was previously not possible to decouple any PCTB sealing issues stemming from the ball valve assembly from those thought to be from the old upper section in the PCTB Mk. 3. Understanding the sensitivity of the ball valve assembly to grit lead to a reinterpretation of the UT-GOM2-1 results. UT-GOM2-1 late sealing is now interpreted to result from temporary jamming of the ball valve mechanism until any ingress of grit is dislodged by the rattling of the core barrel as it is raised to the surface. The PCTB Land Test II illuminated that failure of the bottom section to seal the autoclave and capture the boost is due to grit and cuttings becoming entrained between the ball valve assembly and outer housing, jamming the seal carrier and/or the ball follower.

To confirm and resolve this failure mode, it was necessary to be able to systematically recreate the conditions wherein sediments jammed the ball-valve mechanism. Geotek began explore this immediately at the Geotek testing facility in Salt Lake City, UT. At the same time, Geotek and Pettigrew Engineering began to explore possible design changes to improve sealing in the presence of mud with cuttings. Post-PCTB Land Test II ball - valve testing and results are discussed in Section 3.6.4 Other: Post-Land Test Evaluation, Testing, and Modification.

PCTB Land Test II: PDT/T2P Tests

During the PCTB Land Test II, at the end of the PCTB testing program, the Probe Deployment Tool (PDT) was deployed in the borehole with the T2P penetrometer. The PDT had not yet been tested in a borehole setting and the T2P's logging electronics have been overhauled since its last deployment.

During the descent, the PDT prematurely released from the Running/Pulling Tool (RPT), and the PDT/T2P fell to rest in the BHA. The PDT/T2P was recovered with an emergency pulling tool. Further testing was not conducted.

Upon recovering the PDT/T2P, we determined that the detents (catches) on the PDT sheared, causing the PDT to detach from the RPT while still in the locked position. This is attributed to higher than expected impact loading. It was determined that upgrades to detent material and the design of surrounding components (latch dogs) would be needed prior to field deployment.

The T2P tip (2 cm) was sheared off at some point in the fall. The T2P appeared otherwise undamaged. The T2P's pressure and temperature data could not be recovered from the test. The new data acquisition system within the T2P appeared to be undamaged, but no data file was found after the test. The cause of failure to record data during this test is being investigated by UT and Leeman Geophysical.

3.6.4 Other: Post-Land Test Evaluation, Testing, and Modification

Following the PCTB Land Test II (Subtask 14.3: PCTB Land Test II) Geotek transported the PCTB Mk. 4 to the Geotek testing facility in Salt Lake City, Utah (Figure 3-21) to investigate the PCTB ball-valve failure modes observed during the PCTB Land Test II.

Figure 3-21: Geotek testing facility in Salt Lake City, Utah. A. Wireline unit and pressurized test well. B. Isolated ball valve assembly for dry fire testing. C. Acrylic test fixture.

Geotek developed an approach to evaluate the interpretation that the PCTB ball valve failure is caused by foreign particles (grit and fine sand) becoming lodged in the seal carrier and ball follower, causing the ball valve to fail upon actuation. Geotek built a test apparatus that enabled visual observation of the PCTB ball valve behavior when actuated. Ball valve actuation tests were then conducted, and were filmed on video at 240 fps and evaluated in slow motion playback. Geotek conducted tests using water and mud loaded with the same concentration and grain sizes of grit that were measured in the drilling mud at CTTF.

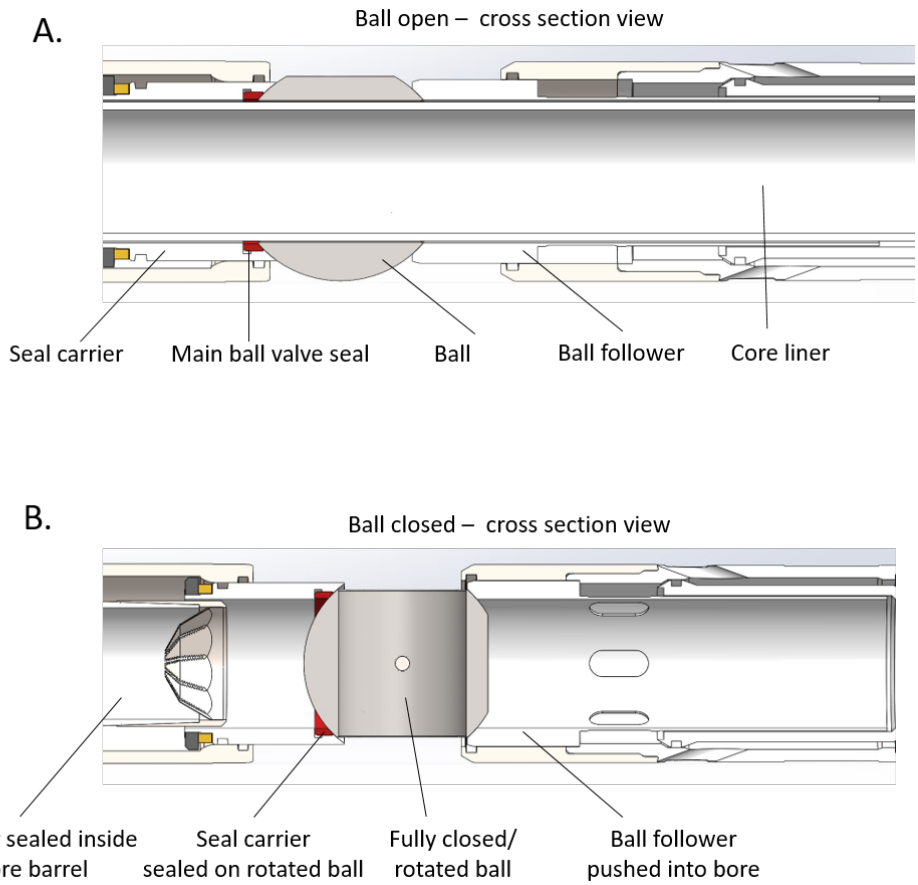

Figure 3-22. Cross sectional view of the PCTB ball valve assembly. A. PCTB ball valve assembly in the open position. B. PCTB ball valve assembly in the closed position.

Geotek was able to achieve grit-induced ball valve failure on a repeatable basis and was able to observe and analyze the effect through the ball valve test chamber. The ball-valve actuation tests confirmed the interpreted results of the PCTB Land Test II: the primary cause of sealing failure is the jamming of the ball follower and the seal carrier due to grit suspended in drilling fluids.

Geotek incrementally developed provisional design solutions to address this problem, and manufactured parts for tests. Geotek then designed procedures to test each modification individually. This iterative process of ball valve actuation testing, remedial design, modification, and further testing continued from March through September, 2020.

The following issues were identified by Geotek as increasing the susceptibility of ball-valve jamming in the current version of the PCTB (PCTB Mk 4):

1. Jamming from fine grit between sliding surface (seal carrier and ball valve housing, ball follower and ball valve housing, and cutting shoe sleeve and ball follower.
2. Flow paths streamline fine grit particles into sliding surfaces
3. Insufficient flow through housing extension to prevent bit balling of cutting shoe ports
4. No cleaning or protection mechanism to prevent jamming
5. Centralization problems allow for seal carrier misalignment during actuation

6. Over-compressed ball valve return spring contributes to jamming
7. Geotek developed provisional design solutions to this problem, and manufactured parts for tests. Geotek then designed a procedure to test each modification individually.

Geotek designed, fabricated, and incrementally tested the proposed upgrades to the PCTB (PCTB Mk 5):

1. Extended seal carrier shoulder for improved centralization during actuation
2. One low friction lip seal on seal carrier
3. Seal carrier and ball follower wiper ring for diverting grit and cleaning surfaces during actuation
4. Extended ball follower shoulder for maintaining contact with wiper ring during actuation
5. Milled slots in ball follower for fluid compensation to prevent hydro locking
6. Short ball valve return spring with fewer coils to prevent jamming
7. Extended cutting shoe sleeve for repositioning of diversion seal
8. Used Polypack seal to divert flow away from sliding surfaces into ports
9. Steeper angled flow ports on housing extension for improved flow paths to cutting shoe flow ports

In early September, 2020, Geotek completed a proof-of-concept PCTB assembly that included all of the PCTB Mk 5 upgrades. On September 29-30, 2020, Geotek conducted a series of demonstration tests with Pettigrew Engineering in attendance. Isolated ball valve tests were performed with two different ball valve assemblies. The first ball valve assembly was the Mk. 4 version of the tool, used during the PCTB Land Test II. The second ball valve assembly used was the Mk. 5 version which includes the design upgrades intended to eliminate the ball-valve failures observed in the PCTB Land Test II. Each test included a water and grit solution with two different quantities of fine grit (53-125 µm particle size). The first quantity of grit uses 0.05 lbs of fine grit per 2.5 gallons of water. This ratio was identical to the 0.24% solids by weight extracted from the CTTF 2020 mud samples. The second quantity of grit used was 0.15 lbs of grit per 2.5 gallons of water, this quantity was used to evaluate how well the design modifications could perform in extreme conditions.

Four ball-valve actuation tests were conducted with the PCTB Mk 4. No tests with the PCTB Mk4 were successful. Thirteen ball-valve actuation tests were conducted with the PCTB Mk. 5. Eight of the thirteen PCTB Mk. 5 tests were successful. The Mk. 5 ball valve initially passed three tests, after which Geotek recognized that the wiper ring seals being used were out of spec. The seals were replaced and testing continued. The Mk. 5 ball valve passed 3/3 additional tests using in-spec seals. The Mk. 5 ball valve was then tested in more extreme conditions using 3X the amount of grit observed at CTTF. This group passed 2/4 tests. In each failed Mk. 5 test, the ball valve completed stroke when a small amount of downward pressure was applied or the assembly was rattled.

A final test (test 14) was performed on the PCTB Mk. 5 in the downhole test chamber. The purpose of this test was to validate that there were no issues during full downhole actuation with the modified Mk. 5 ball valve. The results of this test demonstrated successful ball-valve actuation and sealing in the downhole pressure chamber.

A report of the September, 2020 ball valve actuation testing results can be found in *DE-FE0023919 Quarterly Research Performance Progress Report (Period Ending 09/31/20), Attachment B: Ball Valve Actuation Testing Results.*

3.7 Task 15.0: UT-GOM2-2 Scientific Drilling Program Preparations

3.7.1 Subtask 15.3: Permitting for UT-GOM2-2 Scientific Drilling Program

Objectives

The Recipient will initiate all activities as required to prepare documentation for UT-GOM2-2 operational and environmental permits. This will include, but not be limited to, all necessary drilling permit applications, bonds, block leases, hazard site reviews, and specialty engineering studies required in order to gain permissions required to execute the Operational Plan.

Accomplishments

In November, 2019, UT assembled a task team consisting of representatives from UT and Ohio State (the UT-GOM2-2 Permit Team), charged with developing the permits for the UT-GOM2-2 Scientific Drilling Program.

With current funding, UT-GOM2-2 will core two wells at two locations in the Gulf of Mexico. With input from the project Sponsors, the decision was made to permit two additional wells: a logging-while-drilling (LWD) well, and cored well at an up-dip location. This approach will position the project with the ability to drill additional wells and complete more of the original science objectives if additional funding become available prior to execution of the drilling program.

The UT-GOM2-2 Permit Team initiated work on the BOEM Exploration Plan Geology and Geophysical (G&G) chapter. UT and Ohio State held weekly web conferences to work on the G&G for WR313 H002 and WR313 G002, that will be drilled as part of the UT-GOM2-2 Scientific Drilling Program. UT and Ohio State also continued work on the G&G for WR313 F001 and WR313 F002, that will be permitted but may only be drilled if additional funding is available.

Throughout Phase 4, the UT-GOM2-2 Permit Team collaborated with the Science and Core Analysis Team on various technical issues, including:

- The coring plan and core point depths
- Maximum number of cores per well based on processing and storage limitations
- Contingency coring plans to respond to different geological scenarios at possible updip location
- Time, mud, and resources estimates for each well

Throughout Phase 4, the UT-GOM2-2 Permit Team also collaborated with the Operations Team on various technical issues, specifically the development of detailed time, mud, and resource estimates for the 'base-case' scenario of each well, allowance cores, and contingency cases.

Throughout Phase 4, the Permitting Team completed the following components of permit documents:

1. The G&G section of the BOEM Exploration Plan
2. The blowout scenario (conditions required to encounter free gas leg(s) due to trajectory deviation
3. Shallow Hazard Assessment Reports for each proposed UT-GOM2-2 drilling location, pursuant to 30 CFR 250.214(f) and 250.244 (f).

4 PRODUCTS DEVELOPED

4.1 AAPG Special Volume on GC 955, Gulf of Mexico

The first of possibly three AAPG Special Volumes dedicated to the UT-GOM2-1 findings at GC 955, Gulf of Mexico (Figure 4-1) was published in Sept of 2020 (https://pubs.geoscienceworld.org/aapgbull/issue/104/9). The Editors for the Special Volume are Ray Boswell (NETL), Ann Cook (Ohio State), Tim Collet (USGS), and Peter Flemings (UT). The first volume contains seven papers with and introduction from the editors.

Figure 4-1: AAPG Bulletin, Vol. 104 Number 9, September 2020

Table 4-1: AAPG Special Volume on GC 955, Gulf of Mexico, papers and DOI links

No.	Primary Author	Reference
Intro	Boswell	Boswell, R., Collet, T.C., Cook, A.E., Flemings, P.B., 2020, Introduction to Special Issue: Gas Hydrates in Green Canyon Block 955, deep-water Gulf of Mexico: Part I: AAPG Bulletin, v. 104, no. 9, p. 1844-1846, http://dx.doi.org/10.1306/bltnintro062320.
1	Flemings	Flemings, P. B., S. C. Phillips, R. Boswell, T. S. Collett, A. E. Cook, T. Dong, and M. Frye, et al., 2020, Pressure coring a Gulf of Mexico deep-water turbidite gas hydrate reservoir: Initial results from The University of Texas-Gulf of Mexico 2-1 (UT-GOM2-1) Hydrate Pressure Coring Expedition: AAPG Bulletin, v. 104, no. 9, p. 1847-1876, http://dx.doi.org/10.1306/05212019052.
2	Thomas	Thomas, C., S. C. Phillips, P. B. Flemings, M. Santra, H. Hammon, T. S. Collett, and A. Cook, et al., 2020, Pressure-coring operations during The University of Texas-Gulf of Mexico 2-1 (UT-GOM2-1) Hydrate Pressure Coring Expedition in Green Canyon Block 955, northern Gulf of Mexico: AAPG Bulletin, v. 104, no. 9, p. 1877–1901, http://dx.doi.org/10.1306/02262019036.
3	Portnov	Portnov, A., A. E. Cook, M. Heidari, D. E. Sawyer, M. Santra, and M. Nikolinakou, 2020, Salt-driven evolution of a gas hydrate reservoir in Green Canyon, Gulf of Mexico: AAPG Bulletin, v. 104, no. 9, p. 1903–1919, http://dx.doi.org/10.1306/10151818125.
4	Santra	Santra, M., P. B. Flemings, E. Scott, and P. K. Meazell, 2020, Evolution of gas hydrate-bearing deep-water channel-levee system in abyssal Gulf of Mexico: Levee growth and deformation: AAPG Bulletin, v. 104, no. 9, p. 1921–1944, http://dx.doi.org/10.1306/04251918177
5	Phillips	Phillips, S. C., P. B. Flemings, M. E. Holland, P. J. Schultheiss, W. F. Waite, J. Jan, E. G. Petrou, and H. Hammon, 2020, High concentration methane hydrate in a silt reservoir from the deep-water Gulf of Mexico: AAPG Bulletin, v. 104, no. 9, p. 1971–1995, http://dx.doi.org/10.1306/01062018280.
6	Meazell	Meazell, K., P. Flemings, M. Santra, and J. E. Johnson, 2020, Sedimentology and stratigraphy of a deep-water gas hydrate reservoir in the northern Gulf of Mexico: AAPG Bulletin, v. 104, no. 9, p. 1945–1969, http://dx.doi.org/10.1306/05212019027.
7	Fang	Fang, Y., P. B. Flemings, H. Daigle, S. C. Phillips, P. K. Meazell, and K. You, 2020, Petrophysical properties of the Green Canyon Block 955 hydrate reservoir inferred from reconstituted sediments: Implications for hydrate formation and production: AAPG Bulletin, v. 104, no. 9, p. 1997–2028, http://dx.doi.org/10.1306/01062019165.

4.2 UT-GOM2-1 Scientific Report

UT worked with the Science Party and UTIG staff to publish the UT-GOM2-1 expedition scientific volume. Chapters were posted on OSIT and new data reports were generated and published on the expedition website (https://ig.utexas.edu/energy/genesis-of-methane-hydrate-in-coarse-grained-systems/expedition-ut-gom2-1/reports/) and on OSTI (https://www.osti.gov/search/semantic:UT-GOM2-1). Table 4-2 presents the volume structure with links.

Table 4-2: UT-GOM2-1 Scientific Volume

Expedition Volume	https://dx.doi.org/10.2172/1646019
Expedition Scientists	https://ig.utexas.edu/energy/genesis-of-methane-hydrate-in-coarse-grained-systems/expedition-ut-gom2-1/expedition-scientists/
Prospectus	http://www-udc.ig.utexas.edu/gom2/UT-GOM2-1%20Prospectus.pdf
Chapter 1. Expedition Summary	https://dx.doi.org/10.2172/1647223
Chapter 2. Expedition Methods	https://dx.doi.org/10.2172/1647226
Chapter 3. Hole GC 955 H002	https://dx.doi.org/10.2172/1648313
Chapter 4. Hole GC 955 H005	https://dx.doi.org/10.2172/1648318
Data Report: High-Resolution Microscopy Images of Sediments from Green Canyon Block 955, Gulf of Mexico	https://dx.doi.org/10.2172/1648312
Data Report: X-Ray Diffraction of Sediments from Green Canyon Block 955, Gulf of Mexico	https://dx.doi.org/10.2172/1648308
Data Report: X-Ray Powder Diffraction	https://dx.doi.org/10.2172/1648320
Data Report: Prestack Waveform Inversion at GC 955: Trials and sensitivity of PWI to high-resolution seismic data	http://dx.doi.org/10.2172/1647733
Data Directory	Index of /gom2 (utexas.edu)

4.3 Publications

Project publications webpage: https://ig.utexas.edu/energy/gom2-methane-hydrates-at-the-university-of-texas/gom2-publications/

Boswell, R., Collet, T.C., Cook, A.E., Flemings, P.B., 2020, Introduction to Special Issue: Gas Hydrates in Green Canyon Block 955, deep-water Gulf of Mexico: Part I: AAPG Bulletin, v. 104, no. 9, p. 1844-1846, http://dx.doi.org/10.1306/bltnintro062320.

Chen, X., and Espinoza, D. N., 2018a, Ostwald ripening changes the pore habit and spatial variability of clathrate hydrate: Fuel, v. 214, p. 614-622. https://doi.org/10.1016/j.fuel.2017.11.065

Chen, X., Verma, R., Espinoza, D. N., and Prodanović, M., 2018, Pore‐Scale Determination of Gas Relative Permeability in Hydrate‐Bearing Sediments Using X‐Ray Computed Micro‐Tomography and Lattice Boltzmann Method: Water Resources Research, v. 54, no. 1, p. 600-608. https://doi.org/10.1002/2017wr021851

Chen, X. Y., and Espinoza, D. N., 2018b, Surface area controls gas hydrate dissociation kinetics in porous media: Fuel, v. 234, p. 358-363. https://doi.org/10.1016/j.fuel.2018.07.030

Cook, A. E., and Portnov, A., 2019, Gas hydrates in coarse-grained reservoirs interpreted from velocity pull up: Mississippi Fan, Gulf of Mexico: COMMENT: Geology, v. 47, no. 3, p. e457-e457. https://doi.org/10.1130/g45609c.1

Cook, A. E., and Sawyer, D. E., 2015, The mud-sand crossover on marine seismic data: Geophysics, v. 80, no. 6, p. A109-A114. https://doi.org/10.1190/geo2015-0291.1

Cook, A. E., and Waite, W. F., 2018, Archie's Saturation Exponent for Natural Gas Hydrate in Coarse-Grained Reservoirs, v. 123, no. 3, p. 2069-2089. https://doi.org/10.1002/2017jb015138

Darnell, K. N., and Flemings, P. B., 2015, Transient seafloor venting on continental slopes from warming-induced methane hydrate dissociation: Geophysical Research Letters, p. n/a-n/a. https://doi.org/10.1002/2015GL067012

Darnell, K. N., Flemings, P. B., and DiCarlo, D., 2019, Nitrogen‐Driven Chromatographic Separation During Gas Injection Into Hydrate‐Bearing Sediments: Water Resources Research. https://doi.org/10.1029/2018wr023414

Ewton, E., 2019, The effects of X-ray CT scanning on microbial communities in sediment coresHonors]: Oregon State University, 21 p.

Fang, Y., Flemings, P. B., Daigle, H., Phillips, S. C., Meazell, P. K., and You, K., 2020, Petrophysical properties of the Green Canyon block 955 hydrate reservoir inferred from reconstituted sediments: Implications for hydrate formation and production: AAPG Bulletin, v. 104, no. 9, p. 1997–2028, https://doi.org/10.1306/01062019165

Flemings, P. B., Phillips, S. C., Boswell, R., Collett, T. S., Cook, A. E., Dong, T., Frye, M., Guerin, G., Goldberg, D. S., Holland, M. E., Jang, J., Meazell, K., Morrison, J., O'Connell, J., Pettigrew, T., Petrou, E., Polito, P. J., Portnov, A., Santra, M., Schultheiss, P. J., Seol, Y., Shedd, W., Solomon, E. A., Thomas, C., Waite, W. F., and You, K., 2020, Pressure coring a Gulf of Mexico Deepwater Turbidite Gas Hydrate Reservoir: Initial results from the UT-GOM2-1 hydrate pressure coring expedition: AAPG Bulletin, v. 104, no. 9, p. 1847-1876. https://doi.org/10.1306/05212019052

Flemings, P. B., Phillips, S. C., Collett, T., Cook, A., Boswell, R., and Scientists, U.-G.-E., 2018, UT-GOM2-1 Hydrate Pressure Coring Expedition Summary, *in* Flemings, P. B., Phillips, S. C., Collett, T., Cook, A., Boswell, R., and Scientists, U.-G.-E., eds., UT-GOM2-1 Hydrate Pressure Coring Expedition Report: Austin, TX, University of Texas Institute for Geophysics.

Hillman, J. I. T., Cook, A. E., Daigle, H., Nole, M., Malinverno, A., Meazell, K., and Flemings, P. B., 2017a, Gas hydrate reservoirs and gas migration mechanisms in the Terrebonne Basin, Gulf of Mexico: Marine and Petroleum Geology, v. 86, no. Supplement C, p. 1357-1373. https://doi.org/10.1016/j.marpetgeo.2017.07.029

Hillman, J. I. T., Cook, A. E., Sawyer, D. E., Küçük, H. M., and Goldberg, D. S., 2017b, The character and amplitude of 'discontinuous' bottom-simulating reflections in marine seismic data: Earth and Planetary Science Letters, v. 459, p. 157-169. https://doi.org/10.1016/j.epsl.2016.10.058

MacLeod, D.R., 2020. Characterization of a silty methane-hydrate reservoir in the Gulf of Mexico: Analysis of full sediment grain size distributions. M.S. Thesis, pp. 165, University of New Hampshire, Durham NH, U.S.A.

Majumdar, U., and Cook, A. E., 2018, The Volume of Gas Hydrate - Bound Gas in the Northern Gulf of Mexico: Geochemistry, Geophysics, Geosystems, v. 19, no. 11, p. 4313-4328. https://doi.org/10.1029/2018gc007865

Majumdar, U., Cook, A. E., Shedd, W., and Frye, M., 2016, The connection between natural gas hydrate and bottom-simulating reflectors: Geophysical Research Letters. https://doi.org/10.1002/2016GL069443

Meazell, K., Flemings, P., Santra, M., and Johnson, J. E., 2020, Sedimentology and stratigraphy of a deepwater gas hydrate reservoir in the northern Gulf of Mexico: AAPG Bulletin, v. 104, no. 9, p. 1945–1969, https://doi.org/10.1306/05212019027

Meyer, D. W., 2018, Dynamics of gas flow and hydrate formation within the hydrate stability zone [Doctor of Philosophy: The University of Texas at Austin.

Meyer, D. W., Flemings, P. B., and DiCarlo, D., 2018a, Effect of Gas Flow Rate on Hydrate Formation Within the Hydrate Stability Zone: Journal of Geophysical Research-Solid Earth, v. 123, no. 8, p. 6263-6276. https://doi.org/10.1029/2018jb015878

Meyer, D. W., Flemings, P. B., DiCarlo, D., You, K. H., Phillips, S. C., and Kneafsey, T. J., 2018b, Experimental Investigation of Gas Flow and Hydrate Formation Within the Hydrate Stability Zone: Journal of Geophysical Research-Solid Earth, v. 123, no. 7, p. 5350-5371. https://doi.org/10.1029/2018jb015748

Moore, M., Phillips, S., Cook, A.E. and Darrah, T., (2020) Improved sampling technique to collect natural gas from hydrate-bearing pressure cores. Applied Geochemistry, Volume 122, November 2020, p. 104773, https://doi.org/10.1016/j.apgeochem.2020.104773.

Phillips, S. C., Flemings, P. B., Holland, M. E., Schulthiss, P. J., Waite, W. F., Jang, J., Petrou, E. G., and H., H., 2020, High concentration methane hydrate in a silt reservoir from the deep-water Gulf of Mexico: AAPG Bulletin, v. 104, no. 9, p. 1971–1995. https://doi.org/10.1306/01062018280

Phillips, S. C., Flemings, P. B., You, K., Meyer, D. W., and Dong, T., 2019, Investigation of in situ salinity and methane hydrate dissociation in coarse-grained sediments by slow, stepwise depressurization: Marine and Petroleum Geology, v. 109, p. 128-144. https://doi.org/10.1016/j.marpetgeo.2019.06.015

Portnov, A., Santra, M., Cook., A.E., and Sawyer, D.E, (in press) The Jackalope gas hydrate system in the northeastern Gulf of Mexico. Journal of Marine and Petroleum Geology. https://doi.org/10.1016/j.marpetgeo.2019.08.036.

Portnov, A., Cook, A. E., Heidari, M., Sawyer, D. E., Santra, M., and Nikolinakou, M., 2020, Salt-driven evolution of a gas hydrate reservoir in Green Canyon, Gulf of Mexico: AAPG Bulletin, v. 104, no. 9, p. 1903–1919, http://dx.doi.org/10.1306/10151818125

Portnov, A., Cook, A. E., Sawyer, D. E., Yang, C., Hillman, J. I. T., and Waite, W. F., 2019, Clustered BSRs: Evidence for gas hydrate-bearing turbidite complexes in folded regions, example from the Perdido Fold Belt, northern Gulf of Mexico: Earth and Planetary Science Letters, v. 528. https://doi.org/10.1016/j.epsl.2019.115843

Santra, M., Flemings, P., Meazell, K., and Scott, E., 2020, Evolution of Gas Hydrate-bearing Deepwater Channel-Levee System in Abyssal Gulf of Mexico – Levee Growth and Deformation: : AAPG Bulletin, v. 104, no. 9, p. 1921–1944, https://doi.org/10.1306/04251918177

Sawyer, D. E., Mason, R. A., Cook, A. E., and Portnov, A., 2019, Submarine Landslides Induce Massive Waves in Subsea Brine Pools: Scientific Reports, v. 9, no. 1, p. 128. https://doi.org/10.1038/s41598-018-36781-7

Sheik, C. S., Reese, B. K., Twing, K. I., Sylvan, J. B., Grim, S. L., Schrenk, M. O., Sogin, M. L., and Colwell, F. S., 2018, Identification and Removal of Contaminant Sequences From Ribosomal Gene Databases: Lessons From the Census of Deep Life: Front Microbiol, v. 9, p. 840. https://doi.org/10.3389/fmicb.2018.00840

Smart, K (2018). Modeling Well Log Responses in Hydrate Bearing Silts. Ohio State University. Undergraduate Thesis.

Smith, A. J., Flemings, P. B., Liu, X., and Darnell, K., 2014, The evolution of methane vents that pierce the hydrate stability zone in the world's oceans: Journal of Geophysical Research: Solid Earth, p. 2013JB010686. https://doi.org/10.1002/2013JB010686

Thomas, C., Phillips, S. C., Flemings, P. B., Santra, M., Hammon, H., Collett, T. S., Cook, A., Pettigrew, T., Mimitz, M., Holland, M., and Schultheiss, P., 2020, Pressure-coring operations during the University of Texas Hydrate Pressure Coring Expedition, UT-GOM2-1, in Green Canyon Block 955, northern Gulf of Mexico: AAPG Bulletin, v. 104, no. 9, p. 1877–1901. https://doi.org/10.1306/02262019036

Wei, L., Cook, A., Daigle, H., Malinverno, A., Nole, M., and You, K., 2019, Factors Controlling Short‐Range Methane Migration of Gas Hydrate Accumulations in Thin Coarse‐Grained Layers: Geochemistry, Geophysics, Geosystems, v. 20, no. 8, p. 3985-4000. https://doi.org/10.1029/2019gc008405

You, K., and Flemings, P. B., 2018, Methane hydrate formation in thick sandstones by free gas flow: Journal of Geophysical Research: Solid Earth, v. 123, p. 4582-4600. https://doi.org/10.1029/2018JB015683

You, K., Flemings, P. B., Malinverno, A., Collett, T. S., and Darnell, K., 2019, Mechanisms of Methane Hydrate Formation in Geological Systems: Reviews of Geophysics, v. 0, no. ja. https://doi.org/10.1029/2018rg000638

You, K., Kneafsey, T. J., Flemings, P. B., Polito, P., and Bryant, S. L., 2015, Salinity-buffered methane hydrate formation and dissociation in gas-rich systems: Journal of Geophysical Research: Solid Earth, v. 120, no. 2, p. 643-661. https://doi.org/10.1002/2014JB011190

4.4 Conference Presentations / Abstracts

Colwell, F., Kiel Reese, B., Mullis, M., Buser-Young, J., Glass, J.B., Waite, W., Jang, J., Dai, S., Phillips, S. 2020. Microbial Communities in Hydrate-Bearing Sediments Following Long-Term Pressure Preservation. Presented as a poster at 2020 Gordon Research Conference on Gas Hydrates

Cook. A., Waite, W. F., Spangenberg, E., and Heeschen, K.U., 2018, Petrophysics in the lab and the field: how can we understand gas hydrate pore morphology and saturation? Invited talk presented at the American Geophysical Union Fall Meeting, Washington D.C.

Cook, A.E., and Waite, B., 2016, Archie's saturation exponent for natural gas hydrate in coarse-grained reservoir. Presented at Gordon Research Conference, Galveston, TX.

Cook, A.E., Hillman, J., Sawyer, D., Treiber, K., Yang, C., Frye, M., Shedd, W., Palmes, S., 2016, Prospecting for Natural Gas Hydrate in the Orca & Choctaw Basins in the Northern Gulf of Mexico. Poster presented at American Geophysical Union, Fall Meeting, San Francisco, CA.

Cook, A.E., Hillman, J., & Sawyer, D., 2015, Gas migration in the Terrebonne Basin gas hydrate system. Abstract OS23D-05 presented at American Geophysical Union, Fall Meeting, San Francisco, CA.

Cook, A. E., & Sawyer, D., 2015, Methane migration in the Terrebonne Basin gas hydrate system, Gulf of Mexico. Presented at American Geophysical Union, Fall Meeting, San Francisco, CA.

Chen X., Espinoza, D.N., Tisato, N., and Flemings, P.B., 2018, X-Ray Micro-CT Observation of Methane Hydrate Growth in Sandy Sediments. Presented at the AGU Fall Meeting 2018, Dec. 10–14, in Washington D.C.

Darnell, K., Flemings, P.B., DiCarlo, D.A., 2016, Nitrogen-assisted Three-phase Equilibrium in Hydrate Systems Composed of Water, Methane, Carbon Dioxide, and Nitrogen. Presented at American Geophysical Union, Fall Meeting, San Francisco, CA.

Dong, T., Lin, J. -F., Flemings, P. B., Gu, J. T., Polito, P. J., O'Connell, J., 2018, Pore-Scale Methane Hydrate Formation under Pressure and Temperature Conditions of Natural Reservoirs. Presented to the AGU Fall Meeting 2018, Washington D.C., 10-14 December.

Ewton, E., Klasek, S., Peck, E., Wiest, J. Colwell F., 2019, The effects of X-ray computed tomography scanning on microbial communities in sediment cores. Poster presented at AGU Fall Meeting.

Erica Ewton et al., 2018, The effects of X-ray CT scanning on microbial communities in sediment cores. Poster presented at American Geophysical Union, Fall Meeting, Washington, D.C. OS23D-1657

Espinoza D.N., Chen X., Luo J.S., Tisato N., Flemings P.B., 2010, X-Ray Micro-CT Observation of Methane Hydrate Growth and Dissociation in Sandy Sediments. Presented to the Engineering Mechanics Institute Conference 2019, Pasadena, CA, 19 June.

Fang, Y., et al., 2020, Petrophysical Properties of Hydrate-Bearing Siltstone from UT-GOM2-1 Pressure Cores. Presented at the AAPG virtual Conference, Oct 1, Theme 9: Analysis of Natural Gas Hydrate Systems I & II

Fang, Y., et al., 2018, Permeability, compression behavior, and lateral stress ration of hydrate-bearing siltstone from UT-GOM2-1 pressure core (GC-955 – northern Gulf of Mexico): Initial Results. Poster presented at American Geophysical Union, Fall Meeting, Washington, D.C. OS23D-1650

Fang, Y., Flemings, P.B., Daigle, H., O'Connell, J., Polito, P., 2018, Measure permeability of natural hydrate-bearing sediments using K0 permeameter. Presented at Gordon Research Conference on Gas Hydrate, Galveston, TX. Feb 24- Mar 02, 2018.

Flemings, P.B., et al., 2020 Pressure Coring a Gulf of Mexico Deep-Water Turbidite Gas Hydrate Reservoir: The UT-GOM2-1 Hydrate Pressure Coring Expedition. Presented at the AAPG virtual Conference, Oct 1, Theme 9: Analysis of Natural Gas Hydrate Systems I & II

Flemings, P., Phillips, S., and the UT-GOM2-1 Expedition Scientists, 2018, Recent results of pressure coring hydrate-bearing sands in the deepwater Gulf of Mexico: Implications for formation and production. Talk presented at the 2018 Gordon Research Conference on Natural Gas Hydrate Systems, Galveston, TX, February 24-March 2, 2018.

Fortin, W., 2018, Waveform Inversion and Well Log Examination at GC955 and WR313 in the Gulf of Mexico for Estimation of Methane Hydrate Concentrations. Presented at Gordon Research Conference on Natural Gas Hydrate Systems, Galveston, TX.

Fortin, W., Goldberg, D.S., Küçük, H. M., 2017, Prestack Waveform Inversion and Well Log Examination at GC955 and WR313 in the Gulf of Mexico for Estimation of Methane Hydrate Concentrations. EOS Trans. American Geophysical Union, Fall Meeting, New Orleans, LA.

Fortin, W., 2016, Properties from Seismic Data. Presented at IODP planning workshop, Southern Methodist University, Dallas, TX.

Fortin, W., Goldberg, D.S., Holbrook, W.S., and Küçük, H.M., 2016, Velocity analysis of gas hydrate systems using prestack waveform inversion. Presented at Gordon Research Conference on Natural Gas Hydrate Systems, Galveston, TX.

Fortin, W., Goldberg, D.S., Küçük, H.M., 2016, Methane Hydrate Concentrations at GC955 and WR313 Drilling Sites in the Gulf of Mexico Determined from Seismic Prestack Waveform Inversion. EOS Trans. American Geophysical Union, Fall Meeting, San Francisco, CA.

Goldberg, D., Küçük, H.M., Haines, S., Guerin, G., 2016, Reprocessing of high resolution multichannel seismic data in the Gulf of Mexico: implications for BSR character in the Walker Ridge and Green Canyon areas. Presented at Gordon Research Conference on Natural Gas Hydrate Systems, Galveston, TX.

Hammon, H., Phillips, S., Flemings, P., and the UT-GOM2-1 Expedition Scientists, 2018, Drilling-induced disturbance within methane hydrate pressure cores in the northern Gulf of Mexico. Poster presented at

the 2018 Gordon Research Conference and Seminar on Natural Gas Hydrate Systems, Galveston, TX, February 24-March 2, 2018.

Heber, R., Kinash, N., Cook, A., Sawyer, D., Sheets, J., and Johnson, J.E., 2017, Mineralogy of Gas Hydrate Bearing Sediment in Green Canyon Block 955 Northern Gulf of Mexico. Abstract OS53B-1206 presented at American Geophysical Union, Fall Meeting, New Orleans, LA.

Hillman, J., Cook, A. & Sawyer, D., 2016, Mapping and characterizing bottom-simulating reflectors in 2D and 3D seismic data to investigate connections to lithology and frequency dependence. Presented at Gordon Research Conference, Galveston, TX.

Johnson, J., et al., 2020, Grain Size, TOC, and TS in Gas Hydrate Bearing Turbidite Facies at Green Canyon Site 955, Gulf of Mexico. Presented at the AAPG virtual Conference, Oct 1, Theme 9: Analysis of Natural Gas Hydrate Systems I & II

Johnson, J.E., Phillips, S.C., and Divins, D.L., 2018, Tracking AOM through TOC and Elemental S: Implications for Methane Charge in Gulf of Mexico Marine Sediments. Abstract OS13A-08 presented at 2018 Fall Meeting, AGU, San Francisco, Calif., 14-18 Dec. Oral Presentation

Johnson, J., 2018, High Porosity and Permeability Gas Hydrate Reservoirs: A Sedimentary Perspective. Presented at Gordon Research Conference on Natural Gas Hydrate Systems, Galveston, TX.

Kinash, N. Cook, A., Sawyer, D. and Heber, R., 2017, Recovery and Lithologic Analysis of Sediment from Hole UT-GOM2-1-H002, Green Canyon 955, Northern Gulf of Mexico. Abstract OS53B-1207 presented at American Geophysical Union, Fall Meeting, New Orleans, LA.

Küçük, H.M., Goldberg, D.S, Haines, S., Dondurur, D., Guerin, G., and Çifçi, G., 2016, Acoustic investigation of shallow gas and gas hydrates: comparison between the Black Sea and Gulf of Mexico. Presented at Gordon Research Conference on Natural Gas Hydrate Systems, Galveston, TX.

Liu, J. et al., 2018, Pore-scale CH4-C2H6 hydrate formation and dissociation under relevant pressure-temperature conditions of natural reservoirs. Poster presented at American Geophysical Union, Fall Meeting, Washington, D.C. OS23D-2824

Malinverno, A., Cook, A. E., Daigle, H., Oryan, B., 2017, Methane Hydrate Formation from Enhanced Organic Carbon Burial During Glacial Lowstands: Examples from the Gulf of Mexico. EOS Trans. American Geophysical Union, Fall Meeting, New Orleans, LA.

Malinverno, A., 2016, Modeling gas hydrate formation from microbial methane in the Terrebonne basin, Walker Ridge, Gulf of Mexico. Presented at Gordon Research Conference on Natural Gas Hydrate Systems, Galveston, TX.

Meazell, K., Flemings, P. B., Santra, M., and the UT-GOM2-01 Scientists, 2018, Sedimentology of the clastic hydrate reservoir at GC 955, Gulf of Mexico. Presented at Gordon Research Conference on Natural Gas Hydrate Systems, Galveston, TX.

Meazell, K., & Flemings, P.B., 2016, Heat Flux and Fluid Flow in the Terrebonne Basin, Northern Gulf of Mexico. Presented at American Geophysical Union, Fall Meeting, San Francisco, CA.

Meazell, K., & Flemings, P.B., 2016, New insights into hydrate-bearing clastic sediments in the Terrebonne basin, northern Gulf of Mexico. Presented at Gordon Research Conference on Natural Gas Hydrate Systems, Galveston, TX.

Meazell, K., & Flemings, P.B., 2016, The depositional evolution of the Terrebonne basin, northern Gulf of Mexico. Presented at 5th Annual Jackson School Research Symposium, University of Texas at Austin, Austin, TX.

Meazell, K., 2015, Methane hydrate-bearing sediments in the Terrebonne basin, northern Gulf of Mexico. Abstract OS23B-2012 presented at American Geophysical Union, Fall Meeting, San Francisco, CA.

Moore, M., Darrah, T., Cook, A., Sawyer, D., Phillips, S., Whyte, C., Lary, B., and UT-GOM2-01 Scientists, 2017, The genetic source and timing of hydrocarbon formation in gas hydrate reservoirs in Green Canyon, Block GC955. Abstract OS44A-03 presented at American Geophysical Union, Fall Meeting, New Orleans, LA.

Morrison, J., Flemings, P., and the UT-GOM2-1 Expedition Scientists, 2018, Hydrate Coring in Deepwater Gulf of Mexico, USA. Poster presented at the 2018 Gordon Research Conference on Natural Gas Hydrate Systems, Galveston, TX.

Murphy, Z., et al., 2018, Three phase relative permeability of hydrate bearing sediments. Poster presented at American Geophysical Union, Fall Meeting, Washington, D.C. OS23D-1647

Oryan, B., Malinverno, A., Goldberg, D., Fortin, W., 2017, Do Pleistocene glacial-interglacial cycles control methane hydrate formation? An example from Green Canyon, Gulf of Mexico. EOS Trans. American Geophysical Union, Fall Meeting, New Orleans, LA.

Oti, E., Cook, A., Phillips, S., and Holland, M., 2019, Using X-ray Computed Tomography (XCT) to Estimate Hydrate Saturation in Sediment Cores from UT-GOM2-1 H005, Green Canyon 955 (Invited talk, U11C-17). Presented to the AGU Fall Meeting, San Francisco, CA.

Oti, E., Cook. A., Phillips, S., Holland, M., Flemings, P., 2018, Using X-ray computed tomography to estimate hydrate saturation in sediment cores from Green Canyon 955 Gulf of Mexico. Talk presented at the American Geophysical Union Fall Meeting, Washington D.C.

Oti, E., Cook, A., 2018, Non-Destructive X-ray Computed Tomography (XCT) of Previous Gas Hydrate Bearing Fractures in Marine Sediment. Presented at Gordon Research Conference on Natural Gas Hydrate Systems, Galveston, TX.

Oti, E., Cook, A., Buchwalter, E., and Crandall, D., 2017, Non-Destructive X-ray Computed Tomography (XCT) of Gas Hydrate Bearing Fractures in Marine Sediment. Abstract OS44A-05 presented at American Geophysical Union, Fall Meeting, New Orleans, LA.

Phillips, S.C., et al., 2020, High Concentration Methane Hydrate in a Silt Reservoir from the Deep-Water Gulf of Mexico. Presented at the AAPG virtual Conference, Oct 1, Theme 9: Analysis of Natural Gas Hydrate Systems I & II

Phillips, S.C., Formolo, M.J., Wang, D.T., Becker, S.P., and Eiler, J.M., 2020. Methane isotopologues in a high-concentration gas hydrate reservoir in the northern Gulf of Mexico. Goldschmidt Abstracts 2020. https://goldschmidtabstracts.info/2020/2080.pdf

Phillips, S.C., 2019, Pressure coring in marine sediments: Insights into gas hydrate systems and future directions. Presented to the GSA Annual Meeting 2019, Phoenix, Arizona, 22-25 September. https://gsa.confex.com/gsa/2019AM/meetingapp.cgi/Paper/338173

Phillips et al., 2018, High saturation of methane hydrate in a coarse-grained reservoir in the northern Gulf of Mexico from quantitative depressurization of pressure cores. Poster presented at American Geophysical Union, Fall Meeting, Washington, D.C. OS23D-1654

Phillips, S.C., Flemings, P.B., Holland, M.E., Schultheiss, P.J., Waite, W.F., Petrou, E.G., Jang, J., Polito, P.J., O'Connell, J., Dong, T., Meazell, K., and Expedition UT-GOM2-1 Scientists, 2017, Quantitative degassing of gas hydrate-bearing pressure cores from Green Canyon 955. Gulf of Mexico. Talk and poster

presented at the 2018 Gordon Research Conference and Seminar on Natural Gas Hydrate Systems, Galveston, TX, February 24-March 2, 2018.

Phillips, S.C., Borgfedlt, T., You, K., Meyer, D., and Flemings, P., 2016, Dissociation of laboratory-synthesized methane hydrate by depressurization. Poster presented at Gordon Research Conference and Gordon Research Seminar on Natural Gas Hydrates, Galveston, TX.

Phillips, S.C., You, K., Borgfeldt, T., Meyer, D.W., Dong, T., Flemings, P.B., 2016, Dissociation of Laboratory-Synthesized Methane Hydrate in Coarse-Grained Sediments by Slow Depressurization. Presented at American Geophysical Union, Fall Meeting, San Francisco, CA.

Portnov A., et al., 2018, Underexplored gas hydrate reservoirs associated with salt diapirism and turbidite deposition in the Northern Gulf of Mexico. Poster presented at American Geophysical Union, Fall Meeting, Washington, D.C. OS51F-1326

Portnov, A., Cook, A., Heidari, M., Sawyer, D., Santra, M., Nikolinakou, M., 2018, Salt-driven Evolution of Gas Hydrate Reservoirs in the Deep-sea Gulf of Mexico. Presented at Gordon Research Conference on Natural Gas Hydrate Systems, Galveston, TX.

Santra, M., et al., 2020, Gas Hydrate in a Fault-Compartmentalized Anticline and the Role of Seal, Green Canyon, Abyssal Northern Gulf of Mexico. Presented at the AAPG virtual Conference, Oct 1, Theme 9: Analysis of Natural Gas Hydrate Systems I & II

Santra, M., et al., 2018, Channel-levee hosted hydrate accumulation controlled by a faulted anticline: Green Canyon, Gulf of Mexico. Poster presented at American Geophysical Union, Fall Meeting, Washington, D.C. OS51F-1324

Santra, M., Flemings, P., Scott, E., Meazell, K., 2018, Evolution of Gas Hydrate Bearing Deepwater Channel-Levee System in Green Canyon Area in Northern Gulf of Mexico. Presented at Gordon Research Conference and Gordon Research Seminar on Natural Gas Hydrates, Galveston, TX.

Treiber, K, Sawyer, D., & Cook, A., 2016, Geophysical interpretation of gas hydrates in Green Canyon Block 955, northern Gulf of Mexico, USA. Poster presented at Gordon Research Conference, Galveston, TX.

Wei, L. and Cook, A., 2019, Methane Migration Mechanisms and Hydrate Formation at GC955, Northern Gulf of Mexico. Abstract OS41B-1668 presented to the AGU Fall Meeting, San Francisco, CA.

Worman, S. and, Flemings, P.B., 2016, Genesis of Methane Hydrate in Coarse-Grained Systems: Northern Gulf of Mexico Slope (GOM^2). Poster presented at The University of Texas at Austin, GeoFluids Consortia Meeting, Austin, TX.

Yang, C., Cook, A., & Sawyer, D., 2016, Geophysical interpretation of the gas hydrate reservoir system at the Perdido Site, northern Gulf of Mexico. Presented at Gordon Research Conference, Galveston, TX, United States.

You, K., et al., 2020, Coupled Multiphase Flow and Reactive Transport Processes in Gas Hydrate Systems. Presented at Gordon Research Conference on Gas Hydrate, Galveston, TX. Feb 2020.

You, K., et al. 2020, Impact of Coupled Free Gas Flow and Microbial Methanogenesis on the Formation and Evolution of Concentrated Hydrate Deposits. Presented at the AAPG virtual Conference, Oct 1, Theme 9: Analysis of Natural Gas Hydrate Systems I & II

You, K., Flemings, P. B., and Santra, M., 2018, Formation of lithology-dependent hydrate distribution by capillary-controlled gas flow sourced from faults. Poster presented at American Geophysical Union, Fall Meeting, Washington, D.C. OS31F-1864

You, K., and Flemings, P. B., 2018, Methane Hydrate Formation in Thick Marine Sands by Free Gas Flow. Presented at Gordon Research Conference on Gas Hydrate, Galveston, TX. Feb 24- Mar 02, 2018.

You, K., Flemings, P.B., 2016, Methane Hydrate Formation in Thick Sand Reservoirs: Long-range Gas Transport or Short-range Methane Diffusion? Presented at American Geophysical Union, Fall Meeting, San Francisco, CA.

You, K.Y., DiCarlo, D. & Flemings, P.B., 2015, Quantifying methane hydrate formation in gas-rich environments using the method of characteristics. Abstract OS23B-2005 presented at 2015, Fall Meeting, AGU, San Francisco, CA, 14-18 Dec.

You, K.Y., Flemings, P.B., & DiCarlo, D., 2015, Quantifying methane hydrate formation in gas-rich environments using the method of characteristics. Poster presented at 2016 Gordon Research Conference and Gordon Research Seminar on Natural Gas Hydrates, Galveston, TX.

4.5 Websites or other Internet Sites

Project Website:
https://ig.utexas.edu/energy/genesis-of-methane-hydrate-in-coarse-grained-systems/

Project SharePoint:
https://sps.austin.utexas.edu/sites/GEOMech/doehd/teams/

UT-GOM2-1 Website:
https://ig.utexas.edu/energy/genesis-of-methane-hydrate-in-coarse-grained-systems/expedition-ut-gom2-1/

4.6 Other Products

Methane Hydrate: Fire, Ice, and Huge Quantities of Potential Energy:
https://www.youtube.com/watch?v=f1G302BBX9w

Fueling the Future: The Search for Methane Hydrate:
https://www.youtube.com/watch?v=z1dFc-fdah4

UTIG Methane Hydrates:
https://www.youtube.com/watch?v=DXseEbKp5Ak

5 ACRONYMS AND ABBREVIATIONS

A list of acronyms and abbreviations used in this document is presented in Table 5-1.

Table 5-1: List of Acronyms and Abbreviations

ACRONYM	DEFINITION
AAPG	The American Association of Petroleum Geologists
AGU	American Geophysics Union
AIST	National Institute of Advanced Industrial Science and Technology
ANOVA	Analysis of Variance
APL	Ancillary Project Letter
ASTM	American Society for Testing and Materials
BET	Brunauer-Emmett-Teller
BHA	Bottom Hole Assembly
BOEM	Bureau of Ocean Energy Management
CH	Fat Clay
CHNS	Carbon, Hydrogen, Nitrogen, & Sulfur
CL	Lean Clay
CPP	Complimentary Project Proposal
CRS	Constant Rate of Strain
CS	Cutting-Shoe
CT	Computed Tomography
CTTF	Cameron Test and Training Facility
DNA	Deoxyribonucleic Acid
DOE	U.S. Department of Energy
FB	Face-Bit
fbsf	feet below sea floor
GC	Green Canyon
GOM	Gulf of Mexico
GRC	Gordon Research Conference
GRS	Gordon Research Seminar
ISO	Isostatic
JIP	Joint Industry Project
JRFB	*JOIDES Resolution* Facility Board
LDEO	Lamont-Doherty Earth Observatory
LWD	Logging-While-Drilling
MAD	Moisture and Density
mbsf	meters below sea floor
MH	Elastic Silt
MICP	Mercury Injection Capillary Pressure
ML	Silt
MQD	Modified Quantitative Degassing

NEPA	National Environmental Policy Act
NETL	National Energy Technology Laboratory
NPDES	National Pollutant Discharge Elimination System
OCS	Outer Continental Shelf
OH	Organic Silt or Clay with High Liquid Limit
OL	Organic Silt or Clay with Low Liquid Limit
PAT	Pressure Actuation Test
PC	Pressure Core
PCATS	Pressure Core Analysis and Transfer System
PCTB	Pressure Coring Tool with Ball
PDT	Probe Deployment Tool
PFT	Pressure Function Test
PMP	Project Management Plan
PMRS	Pressure Maintenance and Relief System
PNATS	Pressure-Core Nondestructive Analysis Tool
QRPPR	Quarterly Research Performance Progress Report
RNA	Ribonucleic Acid
SEM	Scanning Electron Microscope
SEP	Science Evaluation Panel
SST	Science, Space, & Technology
STC	Schlumberger Technology Corp
T2P	Termperature-2-Pressure Probe
TAG	Technical Advisory Group
TAMU - CC	Texas A&M University, Corpus Christi
TD	Total Depth
TN	Total Nitrogen
TOC	Total Organic Carbon
UNH	University of New Hampshire
UNH	University of New Hampshire
USCS	Unified Soil Classification System
USGS	U.S. Geologic Survey
UT	The University of Texas at Austin
UTIG	UT Institute for Geophysics
UW	University of Washington
WBM	Water-Based Mud
XCT	X-ray Computed Tomography
XRD	X-ray Diffraction

6 BIBLIOGRAPHY

Barry, P. H., Lawson, M., Meurer, W. P., Cheng, A., and Ballentine, C. J., 2018, Noble Gases in Deepwater Oils of the U.S. Gulf of Mexico: Geochemistry, Geophysics, Geosystems, v. 19, no. 11, p. 4218-4235. https://doi.org/10.1029/2018gc007654

Bernard, B. B., Brooks, J. M., and Sackett, W. M., 1976, Natural gas seepage in the Gulf of Mexico: Earth and Planetary Science Letters, v. 31, no. 1, p. 48-54. https://doi.org/10.1016/0012-821X(76)90095-9

Darrah, T. H., Jackson, R. B., Vengosh, A., Warner, N. R., Whyte, C. J., Walsh, T. B., Kondash, A. J., and Poreda, R. J., 2015, The evolution of Devonian hydrocarbon gases in shallow aquifers of the northern Appalachian Basin: Insights from integrating noble gas and hydrocarbon geochemistry: Geochimica et Cosmochimica Acta, v. 170, p. 321-355. https://doi.org/https://doi.org/10.1016/j.gca.2015.09.006

Etiope, G., 2017, Natural Gas, *in* White, W. M., ed., Encyclopedia of Geochemistry: A Comprehensive Reference Source on the Chemistry of the Earth: Cham, Springer International Publishing, p. 1-5.

Fang, Y., Flemings, P. B., Daigle, H., Phillips, S. C., Germaine, J. T., and O'Connell, J. I., Submitted-a, The compression behavior of the hydrate reservoir at Green Canyon Block 955, Gulf of Mexico: AAPG Bulletin.

Fang, Y., Flemings, P. B., Daigle, H., Phillips, S. C., Meazell, K., and You, K., 2020, Petrophysical properties of the Green Canyon Block 955 hydrate reservoir inferred from reconstituted sediments: Implications for hydrate formation and production: AAPG Bulletin, v. 104, no. 9, p. 1997-2028. https://doi.org/10.1306/01062019165

Fang, Y., Flemings, P. B., Daigle, H., Phillips, S. C., and O'Connell, J. I., Submitted-b, Permeability of methane hydrate-bearing sandy silts in the deepwater Gulf of Mexico (Green Canyon Block 955): AAPG Bulletin.

Harkness, J. S., Darrah, T. H., Warner, N. R., Whyte, C. J., Moore, M. T., Millot, R., Kloppmann, W., Jackson, R. B., and Vengosh, A., 2017, The geochemistry of naturally occurring methane and saline groundwater in an area of unconventional shale gas development: Geochimica et Cosmochimica Acta, v. 208, p. 302-334. https://doi.org/https://doi.org/10.1016/j.gca.2017.03.039

Jackson, R. B., Vengosh, A., Darrah, T. H., Warner, N. R., Down, A., Poreda, R. J., Osborn, S. G., Zhao, K., and Karr, J. D., 2013, Increased stray gas abundance in a subset of drinking water wells near Marcellus shale gas extraction: Proceedings of the National Academy of Sciences, p. 201221635. https://doi.org/10.1073/pnas.1221635110

Jenden, P. D., Drazan, D. J., and Kaplan, I. R., 1993, Mixing of Thermogenic Natural Gases in Northern Appalachian Basin: American Association of Petroleum Geologists Bulletin, v. 77, p. 980-998.

McBride, B. C., Weimer, P., and Rowan, M. G., 1998, The effect of allochthonous salt on the petroleum systems of northern Green Canyon and Ewing Bank (offshore Louisiana), northern Gulf of Mexico: AAPG Bulletin, v. 82, no. 5B, p. 1083-1112.

Meazell, K., Flemings, P. B., Santra, M., and Johnson, J. E., 2020, Sedimentology and stratigraphy of a deep-water gas hydrate reservoir in the northern Gulf of Mexico: AAPG Bulletin, v. 104, no. 9, p. 1945-1969. https://doi.org/10.1306/05212019027

Milkov, A., 2011, Wordwide distribution and significance of secondary microbial methane formed during petroleum biodegradation in conventional reservoirs: Organic Geochemistry - ORG GEOCHEM, v. 42, p. 184-207. https://doi.org/10.1016/j.orggeochem.2010.12.003

Milkov, A. V., and Etiope, G., 2018, Revised genetic diagrams for natural gases based on a global dataset of >20,000 samples: Organic Geochemistry, v. 125, p. 109-120. https://doi.org/https://doi.org/10.1016/j.orggeochem.2018.09.002

Moore, M. T., Phillips, S. C., Cook, A. E., and Darrah, T. H., 2020, Improved sampling technique to collect natural gas from hydrate-bearing pressure cores: Applied Geochemistry, v. 122. https://doi.org/10.1016/j.apgeochem.2020.104773

Moore, M. T., Vinson, D. S., Whyte, C. J., Eymold, W. K., Walsh, T. B., and Darrah, T. H., 2018, Differentiating between biogenic and thermogenic sources of natural gas in coalbed methane reservoirs from the Illinois Basin using noble gas and hydrocarbon geochemistry: Geological Society, London, Special Publications, v. 468, no. 1, p. 151-188. https://doi.org/10.1144/sp468.8

Phillips, S. C., Flemings, P. B., Holland, M. E., Schulthiss, P. J., Waite, W. F., Jang, J., Petrou, E. G., and Helen, H., 2020, High concentration methane hydrate in a silt reservoir from the deep-water Gulf of Mexico: AAPG Bulletin, v. 104, no. 9, p. 1971-1995. https://doi.org/10.1306/01062018280

Rebata-Landa, V., and Santamarina, J. C., 2006, Mechanical limits to microbial activity in deep sediments: Geochemistry, Geophysics, Geosystems, v. 7, no. 11. https://doi.org/10.1029/2006gc001355

Sassen, R., Milkov, A. V., Ozgul, E., Roberts, H. H., Hunt, J. L., Beeunas, M. A., Chanton, J. P., DeFreitas, D. A., and Sweet, S. T., 2003, Gas venting and subsurface charge in the Green Canyon area, Gulf of Mexico continental slope: evidence of a deep bacterial methane source?: Organic Geochemistry, v. 34, no. 10, p. 1455-1464. https://doi.org/10.1016/S0146-6380(03)00135-9

Schoell, M., 1980, The hydrogen and carbon isotopic composition of methane from natural gases of various origins: Geochimica et Cosmochimica Acta, v. 44, no. 5, p. 649-661. https://doi.org/doi:10.1016/0016-7037(80)90155-6

-, 1983, Genetic Characterization of Natural Gases1: AAPG Bulletin, v. 67, no. 12, p. 2225-2238. https://doi.org/10.1306/ad46094a-16f7-11d7-8645000102c1865d

Thomas, C., Phillips, S. C., Flemings, P. B., Santra, M., Hammon, H., Collett, T. S., Cook, A. E., Pettigrew, T., Mimitz, M., Holland, M., and Schultheiss, P., 2020, Pressure coring operations during The University of Texas-Gulf of Mexico 2-1 (UT-GOM2-1) Hydrate Pressure Coring Expedition in Green Canyon Block 955, northern Gulf of Mexico: AAPG Bulletin, v. 104, no. 9, p. 1877-1901. https://doi.org/10.1306/02262019036

Vinson, D. S., Blair, N. E., Martini, A. M., Larter, S., Orem, W. H., and McIntosh, J. C., 2017, Microbial methane from in situ biodegradation of coal and shale: A review and reevaluation of hydrogen and carbon isotope signatures: Chemical Geology, v. 453, p. 128-145. https://doi.org/https://doi.org/10.1016/j.chemgeo.2017.01.027

Whiticar, M. J., Faber, E., and Schoell, M., 1986, Biogenic methane formation in marine and freshwater environments: CO2 reduction vs. acetate fermentation—Isotope evidence: Geochimica et Cosmochimica Acta, v. 50, no. 5, p. 693-709. https://doi.org/http://dx.doi.org/10.1016/0016-7037(86)90346-7

National Energy Technology Laboratory

626 Cochrans Mill Road
P.O. Box 10940
Pittsburgh, PA 15236-0940

3610 Collins Ferry Road
P.O. Box 880
Morgantown, WV 26507-0880

1450 Queen Avenue SW
Albany, OR 97321-2198

Arctic Energy Office
420 L Street, Suite 305
Anchorage, AK 99501

Visit the NETL website at:
www.netl.doe.gov

Customer Service Line:
1-800-553-7681

NATIONAL ENERGY TECHNOLOGY LABORATORY

U.S. DEPARTMENT OF ENERGY | NATIONAL ENERGY TECHNOLOGY LABORATORY